

THE CHEMODYNAMICAL EVOLUTION OF THE MILKY WAY DISC I: THE SOLAR VICINITY

I. MINCHEV¹, C. CHIAPPINI¹, M. MARTIG²*Draft version August 9, 2012*

ABSTRACT

In this first paper of this series, we present a new approach for studying the chemodynamical evolution in disc galaxies, which consists of fusing disc chemical evolution models with compatible numerical simulations of galactic discs. Such a method avoids known star formation and chemical enrichment problems encountered in simulations. Here we focus on the Milky Way, by using a detailed thin-disc chemical evolution model (matching local observables, which are weakly affected by radial migration) and a simulation in the cosmological context, with dynamical properties close to those of our Galaxy. We examine in detail the interplay between in-situ chemical enrichment and radial migration, and their impact on key observables in the solar neighborhood, e.g., the age-metallicity-velocity relation, the metallicity distribution, and gradients in the radial and vertical directions. We show that, due to radial migration from mergers at high redshift and the central bar at later times, a sizable fraction of old metal-poor, high- $[\alpha/\text{Fe}]$ stars can reach the solar vicinity. This naturally accounts for a number of observations related to both the thin and thick discs, despite the fact that we use thin-disc chemistry only. Although significant radial mixing is present, a slope in the age-metallicity relation is preserved, with a scatter compatible with recent observational work. While we find a smooth density distribution in the $[\text{O}/\text{Fe}]$ - $[\text{Fe}/\text{H}]$ -plane, we can recover the observed discontinuity by selecting particles according to kinematical criteria used in high-resolution samples to define the thin and thick discs. We show that in the absence of early-on massive mergers the vertical velocity dispersion of the oldest stars is underestimated by a factor of ~ 2 compared to observations. We predict that the most likely birth place for the Sun is in the range $4.4 < r < 7.7$ kpc (for a current location at $r = 8$ kpc), with the highest probability ~ 5.6 kpc, followed by ~ 7 kpc. Finally, we offer a new, unifying model for the Milky Way thick disc, where both mergers and radial migration play a role at different stages of the disc evolution.

Subject headings: ISM: abundances — Galaxy: abundances — galaxies: ISM — Galaxy: evolution — galaxies: kinematics and dynamics — galaxies: structure

1. INTRODUCTION

Crucial information regarding the dominant mechanism responsible for the formation of the Milky Way (MW) disc and other Galactic components, is encoded in the chemical and dynamical properties of its stars. This conviction has led to an unprecedented observational efforts in the past decades, aimed at mapping the chemistry and kinematics of a large number of stars in the MW. Until the end of 2003, most of the information was confined to small local samples, for which high-resolution spectroscopic data was obtained (e.g., Fuhrmann 1998, 2008 within 25 pc and Bensby et al. 2003 within 100 pc). In 2004, the Geneva Copenhagen Survey (CGS Nordström et al. 2004) obtained the first large spectro-photometric sample of around 16 000 stars, as part of a Hipparcos follow-up campaign (hence, also confined to 100 pc from the Sun). More recently, optical spectroscopic low-resolution surveys, such as SEGUE (Yanny and Rockosi 2009) and RAVE (Steinmetz et al. 2006), have extended the studied volume to distances of a few kpc from the Sun (with the majority of stars in the distance range 0.5-3 kpc), and increased the num-

bers of stars with chemo-kinematical information by more than an order of magnitude ($>200\,000$ spectra for SEGUE and $>500\,000$ spectra for RAVE, see Steinmetz 2012). This effort will be soon complemented by high-resolution spectroscopic surveys both in the optical – HERMES (Freeman et al. 2010) and in the near-infrared – APOGEE (Allende Prieto et al. 2008; Majewski et al. 2010). APOGEE aims at measuring chemo-kinematical properties of around 10^5 stars close to the galactic plane, thus complementing SEGUE and RAVE (which exclude most stars below ~ 200 pc), whereas HERMES aims at obtaining chemical information for around 10^6 stars. In the near future, 4MOST (de Jong et al. 2012), probably the most ambitious project, aims at sampling even larger volumes by obtaining chemo-kinematical properties of many millions of stars (taking full advantage of the Gaia astrometric results). The common aim of the huge observational campaigns briefly summarized above is to constrain the MW assembly history – one of the main goals of the newly emerged field, Galactic Archaeology.

The underlying principle of Galactic Archaeology is that the chemical elements synthesized inside stars, and later ejected back into the interstellar medium (ISM), are incorporated into new generations of stars. As different elements are released to the ISM by stars of different masses and, therefore, on different timescales, stellar abundance ratios provide a cosmic clock, capable of eliciting the past history of star formation and gas accretion

¹ Leibniz-Institut für Astrophysik Potsdam (AIP), An der Sternwarte 16, D-14482, Potsdam, Germany; iminchev1@gmail.com

² Centre for Astrophysics & Supercomputing, Swinburne University of Technology, P.O. Box 218, Hawthorn, VIC 3122, Australia

of a galaxy³. One of the most widely used “chemical-clocks” is the $[\alpha/\text{Fe}]$ ratio⁴.

1.1. Galactic Archeology and radial migration

The power of Galactic Archaeology has been threatened both by observational and theoretical results, showing that stars most probably move away from their birthplaces, i.e., migrate radially. Observational signatures of this radial migration (or mixing) have been reported in the literature since the 1970’s, with the pioneering works by Grenon (1972, 1989). Grenon identified an old population of *super-metal-rich stars* (hereafter SMR), presently at the Solar vicinity, but with kinematics and abundance properties indicative of an origin in the inner Galactic disc (see also Castro et al. 1997 and Trevisan et al. 2011). These results were extended by Haywood (2008), who showed, by re-analyzing the GCS data, that the low- and high-metallicity tails of the thin disc are populated by objects, whose orbital properties suggest origin in the outer and inner Galactic disc, respectively. In particular, the so-called SMR stars show metallicities which exceed the present day ISM and those of young stars at the solar vicinity. As discussed by Chiappini et al. (2003) (see also Table 5 by Asplund et al. 2009), the metallicity at the solar vicinity is not expected to increase much since the Sun’s formation, i.e., in the last ~ 4 Gyr, due to the rather inefficient star formation rate (SFR) at the solar radius during this period, combined with continuous gas infall into the disc. Hence, as summarized in Chiappini (2009), pure chemical evolution models for the MW thin disc cannot explain stars more metal rich than ~ 0.2 dex and radial migration has to be invoked.

N-body simulations have also long shown that radial migration is unavoidable. Raboud et al. (1998) studied numerical simulations aimed at explaining the results by Grenon (1989) of a mean positive U-motion (where U is the Galactocentric radial velocity component of stars), which the authors interpreted as metal-rich stars from the inner galaxy, wandering in the solar neighborhood. However, Raboud et al. (1998) interpreted their findings as stars on hot bar orbits, not recognizing that permanent changes to the stellar angular momenta are possible. It was not until the work by Sellwood and Binney (2002) that radial migration was established as an important process affecting the entire disc, where stars shift guiding radii due to interaction with transient spiral structure. Modern, high-resolution simulations (e.g., Roškar et al. 2008, 2011) have confirmed this finding, but left the role of the Galactic bar unexplored.

A different radial migration mechanism was proposed by Minchev and Famaey (2010) and Minchev et al. (2011a), resulting from the non-linear coupling between the bar and spiral waves, or spirals of different multiplicity (Minchev and Quillen 2006; Minchev et al. 2012a). These works, along with studies of diffusion coefficients in barred discs (Brunetti et al. 2011; Shevchenko 2011), predict a variation in migration efficiency with time and

disc radius, establishing that the dynamical influence of the bar plays an integral part of MW disc modeling. Recently, Comparetta and Quillen (2012) showed that radial migration can result from short-lived density peaks arising from interference of spiral density waves, even if patterns are long-lived. Aside from internal structure, perturbations due to minor mergers have also been shown to be effective at mixing the outer discs (Quillen et al. 2009; Bird et al. 2012), but also can, indirectly, affect the entire disc by inducing (reinforcing) spiral and bar instabilities. Considering the established presence of a central bar, spiral structure and evidence for merger activity in the MW, it is clear that all of the above mentioned radial migration mechanisms would have an effect on the Galactic disc.

In summary, a number of both observational and theoretical results challenge the power of Galactic Archaeology. Therefore, the only possible way to advance in this field is the development of chemodynamical models tailored to the MW, in the cosmological framework. Only then, a meaningful comparison with the large amounts of current and forthcoming observational data (as summarized in the beginning of this Sec.), can be carried out. This is the main goal of the present work, namely, to develop a chemodynamical model for the MW, to be able to quantify the importance of radial mixing throughout the evolution of our Galaxy.

1.2. Difficulties with fully self-consistent simulations

Producing disc-dominated galaxies has traditionally been challenging for cosmological models. In early simulations, extreme angular momentum loss during mergers gave birth to galaxies with overly-concentrated mass distributions and massive bulges (e.g., Navarro and Benz 1991; Navarro and White 1994; Abadi et al. 2003). Although an increase in resolution and a better modeling of star formation and feedback have allowed recent simulations to produce MW-mass galaxies with reduced bulge fractions (Agertz et al. 2011; Guedes et al. 2011; Martig et al. 2012), none of these simulations include chemical evolution. Galaxy formation simulations including some treatment of chemical evolution have been performed by several groups (Raiteri et al. 1996; Mosconi et al. 2001; Lia et al. 2002; Kawata and Gibson 2003; Kobayashi 2004; Scannapieco et al. 2005; Martínez-Serrano et al. 2008; Oppenheimer and Davé 2008; Wiersma et al. 2009; Few et al. 2012). However, although the results are encouraging, and global observed trends seem to be reproduced, such as the mass-metallicity relation (e.g., Kobayashi et al. 2007) or the metallicity trends between the different galactic components (e.g., Tissera et al. 2012), it is still a challenge for these simulations to reproduce the properties of the MW (e.g., the typical metallicities of the different components – Tissera et al. 2012). Additionally, the fraction of low metallicity stars are often overestimated (Kobayashi and Nakasato 2011; Calura et al. 2012), and reproducing the position of thin- and thick-disc stars in the $[\text{O}/\text{Fe}]$ - $[\text{Fe}/\text{H}]$ plane has proved challenging (Brook et al. 2012). While such issues could be due to unresolved metal mixing (Wiersma et al. 2009), it is also worth noticing that none of the above-mentioned simulations reproduces simultaneously the mass, the morphology and star formation

³ In most cases, the stellar surface abundances reflect the composition of the interstellar medium at the time of their birth; this is the reason why stars can be seen as fossil records of the Galaxy evolution.

⁴ Here we use the notation in brackets to indicate abundances relative to the Sun, i.e., $[\text{X}/\text{Y}] = \log(\text{X}/\text{Y}) - \log(\text{X}/\text{Y})_{\odot}$.

history (SFH) of the MW.

This situation has led us to look for a novel way to approach this complex problem. We will show that this approach works encouragingly well, explaining not only current observations, but also leading to a more clear picture regarding the nature of the MW thick disc.

1.3. Thick discs formation scenarios

The large uncertainties in important observational constraints in the MW, such as the age-velocity-metallicity relation, abundance gradients and their evolution, together with the inherent complexity of the topic of Galaxy Assembly, have led to different scenarios to be proposed for the formation of the thick disc.

One possibility is that thick discs were born thick at high redshift from the internal gravitational instabilities in gas-rich, turbulent, clumpy discs (Bournaud et al. 2009; Forbes et al. 2012) or in the turbulent phase associated with numerous gas-rich mergers (Brook et al. 2004, 2005). They could also have been created through accretion of galaxy satellites (Meza et al. 2005; Abadi et al. 2003), where thick disc stars then have an extragalactic origin.

Another possibility is that thick discs are created through the heating of preexisting thin discs. This can either happen fast, on a Gyr timescale, in an early violent epoch, or as a continuous process throughout the galaxy lifetime. In the first case, the thick disc would appear as a clear distinct component in chemistry and phase-space, while in the latter case it would rather be seen as a gradual, continuous transition.

Preexisting thin discs can be heated fast through the effect of multiple minor mergers (Quinn et al. 1993; Villalobos and Helmi 2008; Di Matteo et al. 2011), the rate of which decreases with decreasing redshift. Evidence for merger encounters can be seen in structure in phase-space of MW disc stars (e.g., Minchev et al. 2009; Gómez et al. 2012c,a), which could last for as long as ~ 4 Gyr (Gómez et al. 2012b).

Finally, a recently proposed mechanism for the formation of thick discs is radial migration, which we discuss next.

1.4. Radial migration and thick discs

In the past several years there has been a growing conviction that radial migration, driven by transient spirals, can be responsible for the formation of thick discs, by bringing out high-velocity-dispersion stars from the inner disc and the bulge (no need for mergers). This scenario was used, for example, in the analytical model of Schönrich and Binney (2009), where the authors managed to explain the MW thin- and thick-disc characteristics without the need of mergers or any discrete heating processes. Similarly, the increase of disc thickness with time found in the simulation by Roškar et al. (2008) has been attributed to migration in the works by Sales et al. (2009) and Loebman et al. (2011).

However, how exactly radial migration affects disc thickening in dynamical models had not been demonstrated (but only assumed), until the recent work by Minchev et al. (2011b, 2012b). The latter authors showed unambiguously that radial migration driven by

secular⁵ (or internal) evolution has minor effect on disc thickening, mostly beyond 3 disc scale-lengths, thus, resulting in a flared disc⁶. This is due to the conservation of vertical action of migrators, as opposed to the incorrect assumption of vertical energy conservation. While not building up a *kinematical* thick disc (since the effect of outward and inward migrators mostly cancels out), Minchev et al. (2012b) noted that radial migration does contribute to a *chemical* thick disc, in the sense that outward migrators are preferentially deposited at higher distances above the galactic plane, with the converse effect for inward migrators. It can be expected that migration *can* thicken the disc, provided that stars were “preheated”, e.g., either by mergers or being born hot⁷ (both of these are expected at high redshift).

Once again, to advance our understanding of the MW disc formation and evolution, we need to make quantitative estimates of the importance of radial mixing, guided by observational constraints. This implies the need for chemodynamical models making predictions specifically for the solar vicinity, where most of the current observational constraints are found. In Sec. 2 we describe the disc simulation we adopt in the present work and in Sec. 3 we describe our input chemistry. Sec. 4 is devoted to our new approach. Our results are shown in Sec. 5, while a new explanation for the origin of the thick disc can be found in Sec. 7. Here we concentrate on results for the solar vicinity, while results for the whole disc are shown in Paper II of this series. Conclusions are drawn in Sec. 8.

2. A LATE-TYPE DISC GALAXY SIMULATION IN THE COSMOLOGICAL CONTEXT

To properly model the MW, it is crucial to be consistent with some observational constraints at redshift $z = 0$, for example, a flat rotation curve (e.g., Merrifield 1992), a small bulge (e.g., Binney et al. 1997), a central bar of an intermediate size (e.g., Babusiaux and Gilmore 2005), gas to total disc mass ratio of ~ 0.14 at the solar vicinity (e.g., Chiappini et al. 2001, and references therein), and local disc velocity dispersions close to the observed ones (e.g., Lee et al. 2011).

It is clear that cosmological simulations would be the natural framework for a state-of-the-art chemodynamical study of the Milky Way. Unfortunately, as described in Sec. 1.2, a number of star formation and chemical enrichment problems still exist in fully self-consistent simulations. We, therefore, resort to (in our view) the next best thing – a high-resolution simulation in the cosmological context coupled with a pure chemical evolution model (Sec. 3), as described in detail in Sec. 4 below.

The simulation used in this work is part of a suite of numerical experiments first presented by Martig et al.

⁵ The expression “secular evolution” in this case is a misnomer, since in addition to “internal”, it also has the meaning of “slow”. In fact, radial migration happens on a radial epicyclic frequency time-scale, making it a very fast process. We, thus, simply use the term “internal” for the rest of the paper.

⁶ Minchev et al. (2012b) showed that migrators *shrink* (vertically cool) the disc inside the bar’s CR, further contributing to disc flaring. This is related to the predominance of inward migrators at such small radii with a mean action smaller than that of the local population.

⁷ Note that migration efficiency drops with velocity dispersion (Solway et al. 2012).

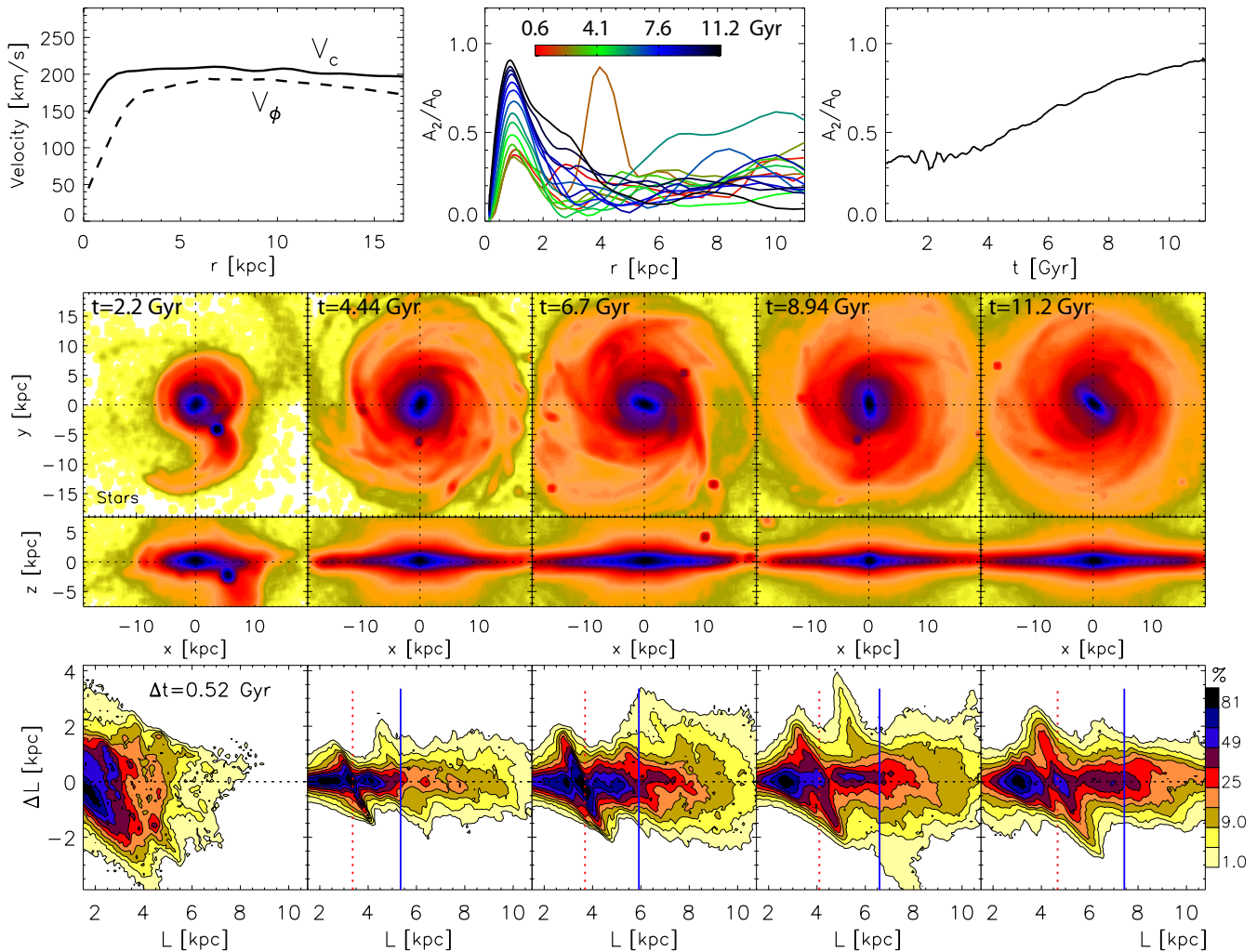


FIG. 1.— **First row:** The left panel shows the rotational velocity (dashed curve) and circular velocity (solid curve) at the final simulation time. The middle panel presents the $m = 2$ Fourier amplitudes, A_2/A_0 , as a function of radius estimated from the stellar density. Curves of different colors present the time evolution of A_2/A_0 . To see better the evolution of the bar strength with time, in the right panel we show the amplitude averaged over the bar maximum. **Second row:** Face-on density maps of the stellar component for different times, as indicated. **Third row:** The corresponding edge-on view. Contour spacing is logarithmic. **Fourth row:** Changes in angular momentum, ΔL , as a function of radius, estimated in a time window of 0.52 Gyr, centered on the times of the snapshots shown above. Both axes are divided by the circular velocity, thus units are kpc (galactic radius). Strong variations are seen with cosmic time due to satellite perturbations and increase in bar strength.

(2012), where the authors studied the evolution of 33 simulated galaxies from $z = 5$ to $z = 0$ using the zoom-in technique described in Martig et al. (2009). This technique consists of extracting merger and accretion histories (and geometry) for a given halo in a Λ -CDM cosmological simulation, and then re-simulating these histories at much higher resolution (150 pc spatial, and $10^{4-5} M_\odot$ mass resolution). The interested reader is referred to Martig et al. (2012) for more information on the simulation method.

The galaxy we have chosen has a number of properties consistent with the MW, including a central bar, as we describe below. We would like to explore the disc evolution for a time period of about 11 Gyr, which is close to the age of the oldest disc stars in the MW. However, none of the above galaxies start forming discs earlier than ~ 9 – 10 Gyr before $z = 0$. To remedy this, we extend our simulation for two additional Gyr, allowing for 11.2 Gyr of self-consistent evolution.

To match the MW in terms of dynamics, we down-

scale the disc radius by a factor of 1.67. This places the bar’s corotation resonance (CR) and 2:1 outer Lindblad resonance (OLR) at ~ 4.7 and ~ 7.5 kpc, respectively, consistent with a number of studies⁸ (e.g., Dehnen 2000, Minchev et al. 2007, 2010, see Gerhard 2011 for a review). At the same time the disc scale-length, measured from particles of all ages in the range $3 < r < 15$ kpc, becomes ~ 3 kpc, in close agreement with observations (e.g., Gerhard 2001). After this change⁹, our simulated disc satisfies the criteria outlined at the beginning of this Section, required for any dynamical study of the MW, in the following:

(i) it has an approximately flat rotation curve with a circular velocity $V_c \sim 210$ km/s at 8 kpc (slightly lower than the MW), shown in the first row, left panel of Fig. 1, where we have corrected for asymmetric drift

⁸ Variations in our results with different rescaling are discussed in the Appendix.

⁹ Note that we rescale the disc radius so as to reflect the position of the bar’s resonances at the final time.

as described in, e.g., Binney and Tremaine (2008).

(ii) the bulge is relatively small, with a bulge-to-total ratio of $\sim 1/5$ (as measured with GALFIT – Peng et al. 2002 – on a mock i-band image, see bottom panel of Fig. 27 by Martig et al. 2012).

(iii) it contains an intermediate size bar at the final simulation time, which develops early on and grows in strength during the disc evolution (see middle and right panels of Fig. 1 and discussion below).

(iv) the disc grows self-consistently as the result of cosmological gas accretion from filaments and (a small number of) early-on gas-rich mergers, as well as merger debris, with a last significant merger concluding $\sim 9-8$ Gyr ago.

(v) the disc gas-to-total mass ratio at the final time is ~ 0.12 , consistent with the estimate of ~ 0.14 for the solar vicinity (Fig. 2, top right panel).

(vi) the radial and vertical velocity dispersions at $r \approx 8$ kpc are ~ 40 and ~ 20 km/s, in very good agreement with observations (see Sec. 5.5 and Fig. 6).

We define $t = 0$ as the time after the central bulge (spheroidal component) has formed. Only about 2% of these stars contribute to the stellar density at the final simulation time in the region $7 < r < 9$ kpc, $|z| < 3$ kpc, which we investigate in this paper. Therefore, for this work we ignore those old stars and focus on the particles forming mostly from gas infall at later times.

In the first row, middle panel of Fig. 1 we plot the Fourier amplitude, A_m/A_0 , of the density of stars as a function of radius, where A_0 is the axisymmetric component and m is the multiplicity of the pattern; here we only show the $m = 2$ component, A_2/A_0 . Different colors indicate the evolution of the A_2 radial profile in the time period specified by the color bar. The bar is seen to extend to $\sim 3-4$ kpc, where deviations from zero beyond that radius are due to spiral structure. The brown curve reaching $A_2/A_0 \sim 0.9$ at $r \approx 4.5$ kpc results from a merger-induced two-armed spiral. To see better the evolution of the bar strength with time, in the right panel we show the amplitude averaged over 1 kpc at the bar maximum.

The second and third rows of Fig. 1 show face-on and edge-on stellar density contours at different times of the disc evolution, as indicated in each panel. The redistribution of stellar angular momentum, L , in the disc as a function of time is shown in the fourth row, where ΔL is the change in the specific angular momentum as a function of radius estimated in a time period $\Delta t = 520$ Myr, centered on the time of each snapshot above. Both axes are divided by the rotational velocity at each radius, therefore L is approximately equal to the initial radius (at the beginning of each time interval) and ΔL gives the distance by which guiding radii change during the time interval Δt . The dotted-red and solid-blue vertical lines indicate the positions of the bar’s CR and OLR. Note that due to the bar’s slowing down, these resonances are shifted outwards in the disc with time.

After the initial bulge formation, the largest merger has a 1:5 stellar-mass ratio and an initially prograde orbit, plunging through the center later and dissolving in ~ 1 Gyr (in the time period $1.5 \lesssim t \lesssim 2.5$ Gyr, first column of Fig. 1). Due to its in-plane orbit (inclination $\lesssim 45^\circ$), this merger event results in accelerated disc growth by triggering strong spiral structure in addition

to its tidal perturbation (Quillen et al. 2009). One can see the drastic effect on the changes in angular momentum, ΔL , in the fourth row, right panel of Fig. 1. More discussion about the importance of this merger can be found in Sections 6.3 and 9.2. A number of less violent events are present at that early epoch, with their frequency decreasing with time. The effect of small satellites, occasionally penetrating the disc at later times, can be seen in the third and fourth columns at $L \approx r \gtrsim 7$ and $L \approx r \approx 6$ kpc, respectively.

We note a strong variation of ΔL with cosmic time, where mergers dominate at earlier times (high z) and internal evolution takes over at $t = 5-6$ Gyr (corresponding to a look-back-time of $\sim 6-7$ Gyr, or $z \sim 1$). The latter is related to an increase with time in the bar’s length and major-to-minor axes ratio as seen in the face-on plots, indicating the strengthening of this structure. Examining the top right panel of Fig. 1, we find a continuous increase in the bar’s $m = 2$ Fourier amplitude with time, where the strongest growth occurs between $t=4$ and 8 Gyr. The effect of the bar can be found in the changes in angular momentum, ΔL , as the feature of negative slope, centered on the CR (dotted-red vertical line), shifting from $L \approx 3.4$ to ≈ 4.7 kpc. Due to the increase in the bar’s amplitude, the changes in stellar guiding radii (vertical axis values) induced by its presence in the CR-region double in the time period $4.44 < t < 11.2$ Gyr (bottom row of Fig. 1). Until recently bars were not considered effective at disc mixing once they were formed, due to their long-lived nature. We emphasize the importance of the bar in its persistent mixing of the inner disc *throughout the galactic evolution* (see Minchev et al. 2012a,b and discussion therein).

3. THE CHEMISTRY

Our new approach is based on a detailed chemical evolution model for the *thin disc only* (essentially the thin disc model presented by Chiappini 2009). The idea behind this is to test if, once radial mixing is taken into account, we can explain the observations of both thin and thick discs without the need of invoking a discrete thick-disc component (different from what was suggested in Chiappini et al. 1997; Chiappini 2009).

In the present model, the thin disc forms mainly via the slow accretion of extragalactic metal-poor gas (assumed to be of primordial composition). We assume the gas accumulates faster in the inner than in the outer regions (similar to what happens in the simulation discussed in Sec. 2). Our code follows in detail a large number of chemical elements by properly taking into account the lifetime of stars of different masses (i.e., we do not use the instantaneous recycling approximation Chiappini et al. 1997). In the present work, we will concentrate only on Iron and Oxygen¹⁰, while other chemical elements will be discussed in the forthcoming papers of this series.

As explained by Chiappini et al. (1997, 2001, 2003), the main observational constraints of MW chemical evolution models are (i) the solar and present day abundances of more than 30 elements, (ii) the current stellar, gas and total mass densities at the solar vicinity (see Fig. 2, upper right panel), (iii) the present SFR

¹⁰ We will often refer to the $[\alpha/\text{Fe}]$ ratios in the text, where in our case Oxygen is the chosen α element.

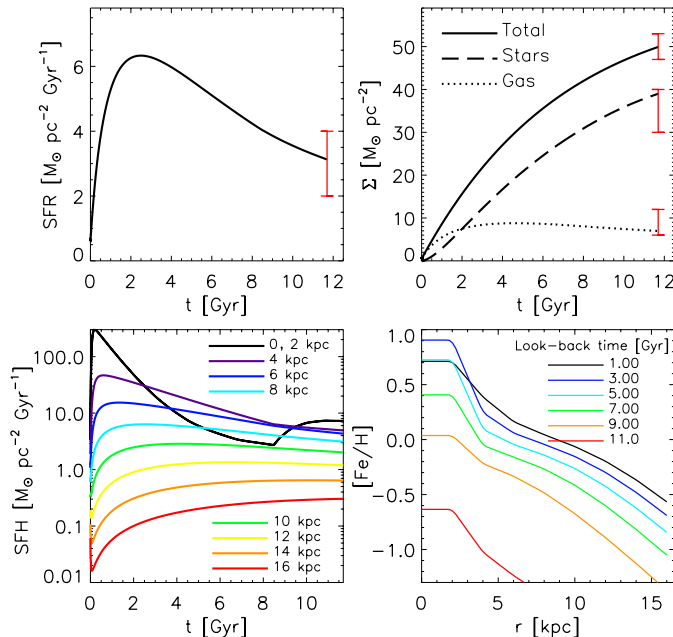


FIG. 2.— Properties of our detailed thin-disc chemical evolution model: **Top, left:** SFR in the solar neighborhood from our thin-disc chemical evolution model. **Top, right:** The total (solid), stellar (dashed) and gas (dotted) density evolution at the solar neighborhood. The error bars are the constraints from observations (see Chiappini et al. 2003, for references to the data). **Bottom, left:** SFR as a function of time; different curves correspond to different radii as indicated. **Bottom, right:** $[\text{Fe}/\text{H}]$ gradients; different curves and colors correspond to different look-back times as indicated.

(see Fig. 2, upper left panel), (iv) the present day supernovae rates of type II and Ia, and (v) the metallicity distribution of G-dwarf stars (to be discussed in Sec. 5). The SFH at the solar vicinity (see Fig. 2, upper left panel) is obtained by assuming a star formation law dependency on the gas density (Kennicutt’s law) and an exponentially decreasing infall with time, with an infall timescale $\tau(R_{g,\odot}) = 7$ Gyr, where $R_{g,\odot} = 8$ kpc is the Sun’s galactocentric distance (see Chiappini 2009, and references therein for details). From the chemical evolution constraints listed above, the one most affected by radial migration is the metallicity distribution¹¹.

Note that this SFH is also in good agreement with the present amount of Deuterium measured in the ISM. The evolution of Deuterium has, apart from its obvious cosmological interest, the role of a very sensitive marker of gas consumption in a given locale. All of the Deuterium in the Universe was created in the Big Bang and none has been released into the ISM ever since, but because it is consumed inside stars, its abundance steadily decreases in direct proportion to the rate of star formation. Thanks to the good knowledge of its primordial value from WMAP, a measure of Deuterium’s present day abundance throughout the Galaxy provides an important direct constraint on the stellar IMF, star formation and infall histories at different locations (as these quantities define the levels of astration of Deuterium in the ISM). The thin disc model used here is similar to the one discussed by Romano et al. (2003, 2006), and more

recently by Lagarde et al. (2012), which well matches the pre-solar and present ISM measurements of D at the solar vicinity.

Outside the solar vicinity, chemical evolution models are mainly constrained by the present day abundance gradients in the thin disc, and are thus more uncertain than the model for the solar vicinity (see discussion in Chiappini et al. 2001). Chiappini et al. (2001) emphasized that the radial abundance gradients predicted along the thin disc, as well as their time evolution, are strongly dependent on pre-enrichment and star formation threshold assumptions. Previous chemical evolution models in the literature considering the thin disc as an independent component could not anticipate such effects. Here we keep it simple by assuming neither threshold nor pre-enrichment; as a consequence, our models predict flattening of the gradients with time, similar to other pure thin-disc chemical evolution models in the literature (e.g. Hou et al. 2001). On the observational side, the question of whether the abundance gradients steepen or flatten with time is still not settled (see Stasińska et al. 2012 for a recent appraisal of the situation).

The chemical gradients we obtain are just a consequence of using different infall timescales at different radii. Here we use the same $\tau(r)$ expression as in Chiappini et al. (2001) down to $r = 2$ kpc. Chemical evolution models are often not computed for the innermost 4 kpc to avoid dealing with the complete lack of observational constraints and with a region where different galactic components co-exist (bulge, bar, and inner disc). As here our main focus is the thin disc, we would like to assign chemistry down to $r = 0$ and will make the conservative hypothesis that the chemistry computed for $r = 2$ kpc applies to all particles with $r < 2$ kpc, as well.

The SFRs at different galactocentric radii are shown at the bottom left panel of Fig. 2. The resulting abundance gradients, for different look-back times, can be found in the bottom right panel of the same figure.

Unfortunately, there are still large uncertainties also in the shape of present-day abundance gradients. From a recent compilation of the best data available in the literature, Stasińska et al. (2012) concluded that most claims of steepening or flattening of the *present* abundance gradients towards the centre or the outskirts of the MW are premature. The only result that seems reliable is the flattening of the disc planetary nebulae abundance gradient towards the centre of the Galaxy, as indicated by the comparison of the works by Chiappini et al. (2009) and Henry et al. (2010). Whether this applies to other abundance gradient tracers is, as of yet, not established (e.g. Pedicelli et al. 2009).

With our current SFH assumptions, the predicted present time gradient, shown by the black curve in the bottom left panel of Fig. 2, amounts to ≈ -0.061 or ≈ -0.057 dex/kpc, depending on the radial range we use for fitting (5-12 or 6-11 kpc, respectively). As we will see, slightly flatter values will be obtained (≈ -0.059 or ≈ -0.058 dex/kpc) once radial migration is taken into account (Sec. 5). It is beyond the scope of the present paper to check for the impact of other assumptions on the abundance gradients, but this will certainly be the focus of a future paper of this series. If the initial gradients turn out to be flatter than the ones adopted here, the effects of radial migration in some observables as the

¹¹ Note that the age-metallicity relation, also affected by radial migration, was never used as a constraint in our chemical evolution models, due to the large scatter shown in the data.

age-metallicity relation will be, of course, weaker than the ones described in Sec. 5.4.

4. A NEW APPROACH FOR COMBINING CHEMISTRY AND DYNAMICS

Despite the recent advances in the general field of galaxy formation and evolution, there are currently no self-consistent simulations, that have the level of chemical implementation required for making detailed predictions for the number of ongoing and planned MW observational campaigns. Even in high-resolution N-body experiments, one particle represents $\sim 10^{4-5}$ solar masses. Hence, a number of approximations are necessary in order to compute the chemical enrichment self-consistently inside a simulation, leading to the several problems briefly discussed in the Introduction. Here, instead, we will assume that each particle is one star¹² and will implement the exact SFH and chemical enrichment from our chemical model (Sec. 3) into our simulated galactic disc (Sec. 2). This can be thought of as inserting the dynamics of our simulation into the chemical model, not the chemistry into the simulation.

We start by dividing the disc into 300-pc radial bins. At each time output we randomly select newly born stars, by matching the SFH corresponding to our chemical evolution model at each radial bin. In case the simulation has formed more stars than needed, those are discarded. If we need more stars at a particular radius and time, we randomly select from the coldest stellar population to emulate the birth kinematics of the required number of extra stars. The particles selected at each time output are assigned the corresponding chemistry for that particular radius and time. This is done recursively at each time-step of 37.5 Myr.

In the just described manner, we follow the self-consistent disc evolution for 11.2 Gyr, selecting a tracer population possessing known SFH and chemistry enrichment. This bypasses all the problems encountered by previous chemodynamical models based on N-body simulations. It also offers a way to easily test the impact of different chemical (or dynamical, see Appendix) prescriptions on the chemodynamical results.

From a chemical point of view, there are two main simplifications in our approach. Firstly, we assume that radial flows do not play a substantial role in the global chemical enrichment of the Galaxy. This seems to be a good approximation as our different chemical evolution zones are 2 kpc wide (see, e.g., Spitoni and Matteucci 2011). Secondly, we assume that stars do not contribute to the chemical evolution outside the zone where they are born, but either contribute only to the chemical enrichment within 2 kpc from their birth place, or never die. This assumption is valid for most of the stars because (i) the massive stars die essentially where they were born, due to their short lifetimes and (ii) low mass stars live longer than the age of the galaxy (never die). We do not expect this simplification to affect our results by more than 10% for chemical elements made in low and intermediate mass stars, and even less for those coming from massive stars, as it is the case for Oxygen.

From a dynamical point of view, the main simplifi-

cations are (i) the resampling of the simulation SFH according to the chemical evolution model and (ii) the difference between the gas-to-total mass ratio expected from the chemical model and attained by the simulation. Although the discs in both the chemical and dynamical models grow inside-out, there are some offsets at particular times. These differences in the SFHs are unavoidable, since the chemical and dynamical models are not tuned to reproduce the same star formation, although they are quite similar for most of the evolution (see also Sec. ??).

As already mentioned in Sec. 2, the disc gas-to-total mass ratio at the final time is ~ 0.12 , consistent with the estimate of ~ 0.14 for the solar vicinity (Fig. 2, top right panel). However, at earlier times the gas fraction at the solar location, for example, can be overestimated by a factor of about 1.5-2 with respect to the chemical model. One effect of a larger gas fraction can be a decreased susceptibility to merger perturbations (e.g., Moster et al. 2010). It may also give rise to a more unstable disc, while suppressing the bar instability (e.g., Bournaud and Combes 2002). Indeed, at earlier times we do find a weaker bar appearing more like a lens, which strengthens later, showing an increase in both its length and major-to-minor axes ratio (Fig. 1). On the other hand, unreasonable disc instabilities due to a large gas fraction in the outer disc are not seen in our simulation. In fact, the spiral structure is about 15% of the background density and does not vary considerably, except when reinforced by mergers at earlier epochs. This amplitude is close to expectations for the MW (e.g., Drimmel and Spergel 2001; Siebert et al. 2012).

While the difference between the assumed (chemical model) and actual (dynamical model) stellar and gas densities can introduce some inconsistencies in the resulting dynamics, this would generally have the tendency of bringing more stars from the inner disc out, due to a larger bar expected at earlier times. As it will become clear later, a larger fraction of old stars coming from the bar's CR region to the solar vicinity would only strengthen our results. Overall, we do not anticipate the simplifications in our approach to affect significantly any of our results. In Sec. 9.1 we perform some tests which support this expectation.

Overall, we do not anticipate the simplifications of our approach to affect significantly any of our results. On the other hand, what we gain with the above simplifications is a new tool to study the chemodynamics of our Galaxy, which is complementary to fully self-consistent models, and where the overall complex problem of galaxy assembly and evolution can be understood by pieces (i.e., same chemistry applied to different simulations and different chemistry applied to the same simulation). We anticipate that this new approach will also be very useful to gain insights that can later be used in fully self-consistent simulations.

5. THE RESULTING CHEMODYNAMICS

After fusing the chemical and dynamical models as outlined above, we are now in a position to (i) look for deviations from the predictions of the purely chemical evolution model and (ii) investigate the causes for these differences.

To first illustrate the migration efficiency in our simulation, in the left panel of Fig. 3 we show the birth radii

¹² Dynamically, this is a good assumption, since the stellar dynamics is collisionless.

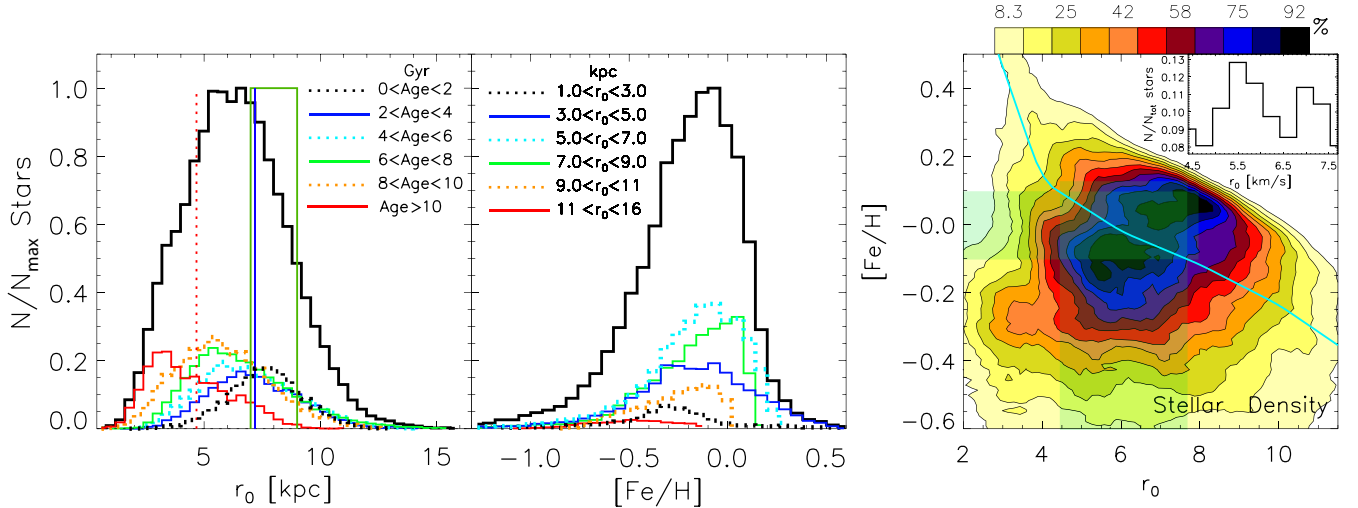


FIG. 3.— **Left:** Birth radii of stars ending up in the “solar” radius (green bin) at the final simulation time. The solid black curve plots the total r_0 -distribution, while the color-coded curves show the distributions of stars in six different age groups, as indicated. The dotted-red and solid-blue vertical lines indicate the positions of the bar’s CR and OLR at the final simulation time. A large fraction of old stars comes from the inner disc, including from inside the CR. **Middle:** $[\text{Fe}/\text{H}]$ distributions for stars ending up in the green bin (left) binned by birth radii in six groups, as indicated. The total distribution is shown by the solid black curve. The importance of the bar’s CR is seen in the large fraction of stars with $3 < r_0 < 5$ kpc (blue line). The cyan curve shows our model solar-age metallicity gradient. Taking an error of ± 1 dex in $[\text{Fe}/\text{H}]$ we find a possible Sun birth radius of $4.6 < r_0 < 7.6$ kpc (where the horizontal green, transparent strip meets the cyan line). The imbedded histogram shows the density of stars in the likely r_0 -range, indicating a decline in the probability for $r_0 \lesssim 5.5$ kpc.

of stars ending up in a solar neighborhood-like location ($7 < r_0 < 9$ kpc, green bin) after 11.2 Gyr of evolution. The bar’s CR and OLR are shown by the dotted-red and solid-blue vertical lines. The solid black line plots the total population, which peaks close to $r_0 = 6$ kpc due to radial migration. An overdensity is seen just inwards of the bar’s CR. The entire sample is also divided into six age-groups, shown by the curves of different colors and line-styles. The strongest effect from radial migration is found for the oldest stars (red curve), whose distribution has a maximum at $r \approx 3$ kpc, or inside the bar’s CR. Note that locally born stars of all ages can be found in the solar neighborhood. A relatively smooth transition of the peak, from older to younger groups of stars, is observed; this is expected, since even for a constant migration efficiency, older stars would be exposed longer to perturbations. While a wide range of birth radii is seen for all age groups, the majority of youngest stars were born at, or close to the solar neighborhood bin.

5.1. The metallicity distribution

The middle panel of Fig. 3 presents the metallicity distribution of stars in our simulated solar neighborhood (green bin in left panel). In addition to the total distribution (solid black line), six subsets of stars, grouped by birth radii, are shown by the different colors and line-styles. The locally born sample (green line) peaks slightly outside $[\text{Fe}/\text{H}] = 0$, ends abruptly at $[\text{Fe}/\text{H}] \sim 0.15$ and has an extended tail toward lower metallicities. This distribution is the same as the one predicted by our pure-thin-disc chemical evolution model with the SFH shown in the top left panel of Fig. 2. Our chemo-dynamical model instead, predicts that the majority of migrators comes from the inner region ($3 < r_0 < 5$ and $5 < r_0 < 7$ kpc bins), as expected. A smaller, but sizable, fraction of stars originating *outside the solar neighborhood* is also observed (orange and red curves).

While the low-metallicity end in the total distribution

comes from contribution by all initial radii, the tail at larger metallicities extending to $[\text{Fe}/\text{H}] \sim 0.6$ results exclusively from stars with $3 < r_0 < 5$ kpc (note that the $5 < r_0 < 7$ kpc bin contributes up to $[\text{Fe}/\text{H}] \sim 0.25$ only). This is the region just inside the bar’s CR, which is where the strongest outward radial migration occurs, as we discussed in Sec. 2 and showed in the bottom row of Fig. 1. At smaller radii stars are trapped in the x_1 bar orbits (e.g., Contopoulos and Papayannopoulos 1980), making outward angular momentum transfer difficult. Nevertheless, stars originating from $1 < r_0 < 3$ kpc still appear in the local bin, with a fraction comparable to that of objects coming from $r_0 > 11$ kpc. We discuss how the metallicity distribution relates to observations in Sec. 6.2 (Fig. 10).

5.2. The birth place of the Sun

With the care taken into defining a proper solar radius in a simulation with MW characteristics, combined with MW chemistry, it is tempting to make an estimate for the solar birth radius, which emerges naturally from our chemodynamical model.

Already from the left panel of Fig. 3 we can see that the age distribution to which the Sun belongs (dotted-cyan curve), suggests a most likely solar birth location at $r \approx 6$ kpc and similar probability of it being born in situ or at $r \approx 5$ kpc. By including the chemical information we can further improve this estimate.

The right panel of Fig. 3 displays density contours of the r_0 - $[\text{Fe}/\text{H}]$ plane for all local stars. The cyan curve shows our input solar-age (4.6 Gyr look-back time) metallicity gradient. Assuming an error of ± 1 dex in $[\text{Fe}/\text{H}]$, we find a possible Sun birth radius in the range $4.4 < r_0 < 7.7$ kpc (where the horizontal green, transparent strip meets the cyan curve).

The imbedded r_0 -histogram in the right panel of Fig. 3 shows the density of stars in the likely r_0 -range, estimated from stars in a narrow age-bin around the solar

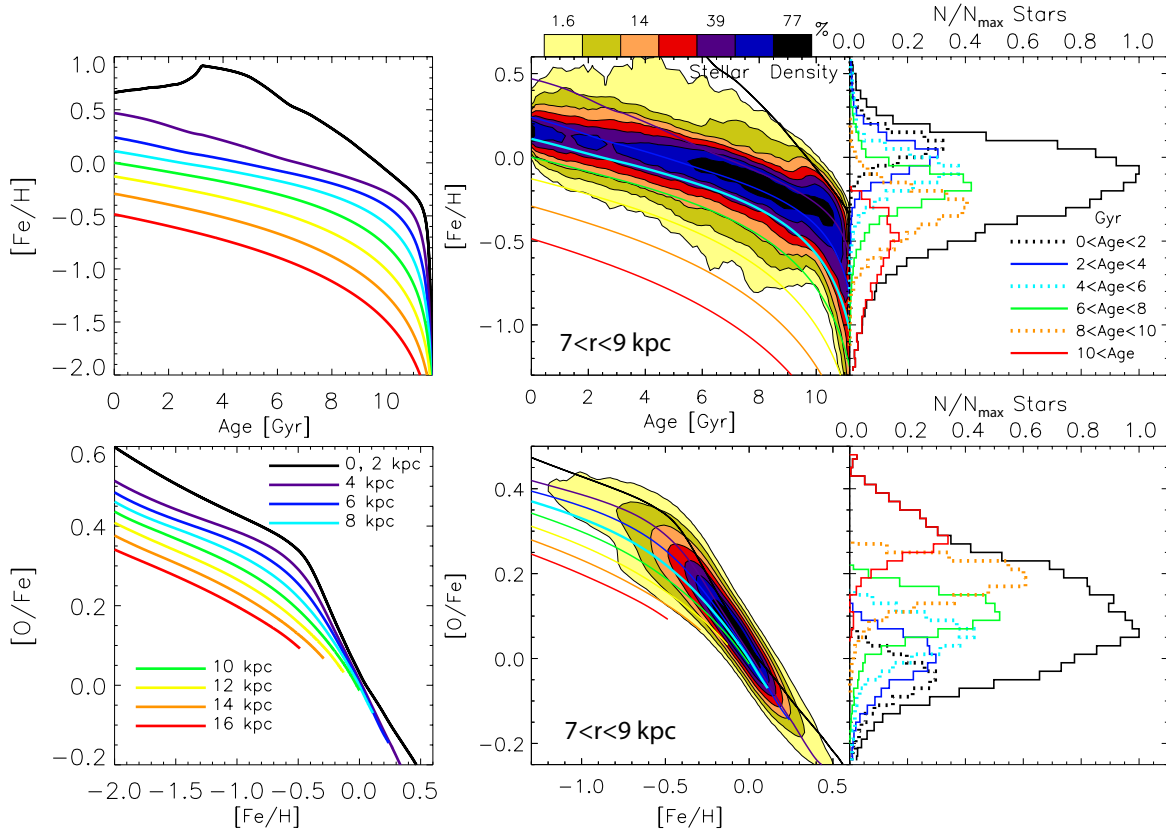


FIG. 4.— **Top:** The left panel plots age versus $[\text{Fe}/\text{H}]$ for different radii, resulting from our input chemical model (left). The middle panel shows stellar density contours of the resulting relation after fusing with dynamics, for the “solar” radius ($7 < r < 9$ kpc). The overlaid lines show the input chemistry for the same radii as in the left. The right panel plots the metallicity distributions for different age bins. **Bottom:** Same as above but for the $[\text{Fe}/\text{H}]-[\text{O}/\text{Fe}]$ relation. There is some contribution from stars born ~ 2 kpc and hardly any from $r > 14$ kpc, consistent with the birth radii distributions shown in Fig. 3.

value (4.6 ± 0.1 Gyr, consistent with, e.g., Bonanno et al. 2002; Christensen-Dalsgaard 2009; Houdek and Gough 2011). We find the highest probability to be around 5.6 kpc, followed by 7 kpc. Note that this estimate is dependent on the migration efficiency in our simulation and the adopted chemical evolution model.

5.3. The age- $[\text{Fe}/\text{H}]$ and $[\text{Fe}/\text{H}]-[\text{O}/\text{Fe}]$ relations

We showed in Figs. 1 (bottom) and 3 (left) that radial mixing is significant in the simulation we use here. It is therefore, very interesting to find out how much the age-metallicity (AMR) and $[\text{Fe}/\text{H}]-[\text{O}/\text{Fe}]$ relations are affected.

To understand better our results, in the first row, left panel of Fig. 4 we show stellar age versus $[\text{Fe}/\text{H}]$ coming from our input chemical model, for different radii, as indicated in the lower panel. The middle panel shows stellar density contours of the resulting relation after fusing with dynamics, for the “solar” radius ($7 < r < 9$ kpc). The overlaid curves highlight the input chemistry for the same radii as in the left, giving an insight about the origin of stars found in this localized bin. We see that stars with $r_0 > 14$ kpc do not enter the solar bin. How much the AMR of locally born stars flattens due to radial migration can be seen by comparing the cyan curve, which corresponds to 8 kpc, to the highest density contours (blue and black). Some flattening is observed, mostly for ages $\gtrsim 5$ Gyr, however the final distribution is by no means flat. The excess of stars at high metallicities is

due to the predominance of migrators coming from the inner disc, as seen in Fig. 3. Similarly, contours below the cyan curve result from stars coming from the outer disc¹³. The bump at age ~ 9.5 Gyr and $[\text{Fe}/\text{H}] \approx -0.1$ results from the strong, merger related migration efficiency at that time (see Sec. 6.3). Identifying such a structure in the observed age-metallicity relation would be indicative of a strong change in the migration efficiency with time (due to the 1:5 mass ratio merger ~ 9 Gyr ago in this case).

The right top panel of Fig. 4 shows the metallicity distributions for different age bins. This is consistent with recent observational results (e.g., Haywood 2012 and references therein), in showing that the scatter in metallicity increases towards older ages. We find the following dispersions in $[\text{Fe}/\text{H}]$ for age groups from young to old: 0.11, 0.14, 0.16, 0.17, 0.15, and 0.7. In all but the oldest bin the distributions appear gaussian. The shape of the red histogram (oldest stars) can be approximated better by a log-normal distribution because of its strong negative skewness. The metallicity peak of this oldest population is around -0.5 , with a range of values in very good agreement with the results by Soubiran et al. (2003) for their thick-disc selection of clump giants. As we found out from Fig. 3, more than 50% of these old stars were

¹³ The deficiency of stars seen at age $\gtrsim 9$ Gyr ($[\text{Fe}/\text{H}] \approx -0.8$) in the lowest density contours is an artifact due to the slightly lower SFR in our simulation at $r > 10$ kpc; note that this only affects a negligibly small number of the oldest stars at this large radius.

born at $r < 5$ kpc. The causes for their outwards migration is discussed in Sec. 6.3.

The bottom row of Fig. 4 is the same as the top one, but for the $[\text{Fe}/\text{H}]-[\text{O}/\text{Fe}]$ relation. The relationship between $[\text{O}/\text{Fe}]$ and age, displayed in the rightmost panel, shows good correlation between the two, assuring that α -elements can be a good age-indicator. However, this figure also shows that the correlation is best seen for older ages. For age $\lesssim 6$ Gyr, the different distributions overlap significantly (see also Fig. 6, bottom). This should be kept in mind when drawing conclusions from large spectroscopic surveys, where often the $[\alpha/\text{Fe}]$ ratio is used as a proxy for age.

By correcting for the spectroscopic sampling of stellar sub-populations in the SEGUE survey, Bovy et al. (2012b) showed recently that the bimodality seen in the $[\text{O}/\text{Fe}]-[\text{Fe}/\text{H}]$ distribution for the uncorrected sample disappears. As the middle bottom panel in Fig. 4 shows, our results are in agreement in that our simulated, unbiased $[\text{O}/\text{Fe}]-[\text{Fe}/\text{H}]$ stellar density distribution is smooth. In Sec. 6.1 we show that biases introduced by the preferential selection of thin- and thick-disc stars, as commonly employed in observations, can result in a gap in the $[\text{O}/\text{Fe}]-[\text{Fe}/\text{H}]$ plane.

5.4. Migration effects on the chemical gradients

In Fig. 5 we show how the initial chemical gradients are affected by the disc dynamics. We divide the galactic disc into six age-bins and plot the $[\text{Fe}/\text{H}]$ and $[\text{O}/\text{Fe}]$ gradients by lines of different colors, as indicated in the bottom panel. Solid and dotted line-styles represent the initial (chemical) and final (chemodynamical) states, respectively. The bar’s CR and OLR (estimated at the end of the simulation) are given by the dotted-red and solid-blue vertical lines, respectively. A strong flattening in $[\text{Fe}/\text{H}]$ is seen for the older populations, however, the younger stars are much less affected. Remarkably, for stars younger than 2 Gyr the final gradient is very similar to the initial one out to ~ 12 kpc. This is related to the fact that the majority of stars in this age-bin are born near their final radii, as we found out was the case for the “solar” radius (see dotted black line in Fig. 3, left). Note that the bar’s CR acts as a pivot point around which the initial metallicity profiles turns counterclockwise, raising values in the disc and lowering them in the bulge/bar region. This is easy to understand by recalling that the bar CR radius is where the strongest exchange of angular momentum occurs (see Fig. 1, bottom row) and is one example of the importance of considering the effect of the bar in modeling the Galactic disc.

To give a quantitative idea for the change in the metallicity gradient of young stars, we fitted lines to the solid (initial) and dotted (final) black lines in Fig. 5, top panel. We estimated that the original gradient of ≈ -0.061 or ≈ -0.057 dex/kpc, depending on the radial range we use for fitting (5–12 or 6–11 kpc, respectively) changes to ≈ -0.059 or ≈ -0.058 dex/kpc at the end of the simulation. This small effect on the gradient of the youngest stellar population is reassuring, since this was used as a constraint for our input chemical evolution model.

Incidentally, it turns out that the CR (which is consistent with what is expected for the MW) is almost exactly at the radius where the input metallicity gradient begins to steepen (Fig. 5, top). While the chemical model we use

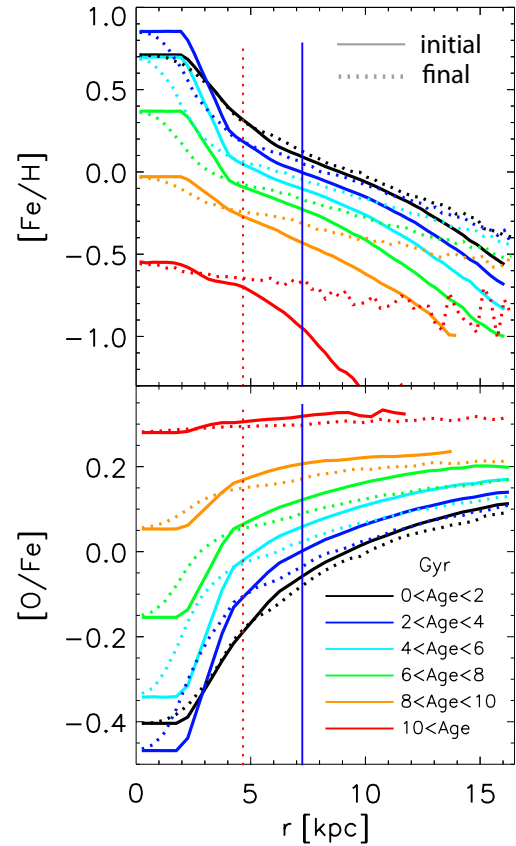


FIG. 5.— The effect on the initial $[\text{Fe}/\text{H}]$ (top) and $[\text{O}/\text{Fe}]$ (bottom) gradients for different stellar age groups. The solid and dotted color curves show the initial and final states, respectively. Note that, while strong flattening is observed for the older populations, the metallicity gradient for the youngest stars (age < 2) is hardly affected at $r \lesssim 12$ kpc, thus justifying the use of our chemical model, which uses this as a constraint.

was not motivated by the effect of the bar and is, in fact, a somewhat extreme case regarding the strong increase in $[\text{Fe}/\text{H}]$ at $r < 5$ kpc, this choice may well be the correct one, considering the stronger chemical enrichment expected inside bars (e.g., Ellison et al. 2011).

Much weaker flattening is seen for the $[\text{O}/\text{Fe}]$ profiles, related to the progressively weaker radial variation of older samples. Due to the reversed gradients compared to $[\text{Fe}/\text{H}]$, a *clockwise* turn is now seen around the CR “pivot point”. In both panels of Fig. 5 the values in the innermost disc region are unaffected. This is because most of these stars are trapped inside the bar, as mentioned above, preventing their escape once the bar is formed.

The prediction that the $[\text{O}/\text{Fe}]$ radial profiles are essentially preserved is an important result and can provide a powerful constraint on different input chemical evolution models. The shapes of the $[\text{O}/\text{Fe}]$ -profiles for different ages bins are a direct consequence of our adopted variation of the infall-law with radius (and hence the SFHs at the different positions). In the near future, these would be possible to measure by combining the good distances and ages expected from the CoRoT mission (Baglin et al. 2006), with abundance ratios obtained by spectroscopic follow-up surveys (see Chiappini 2012; Freeman 2012). For the young populations, this should be already possible to be obtained from the observations of open clusters,

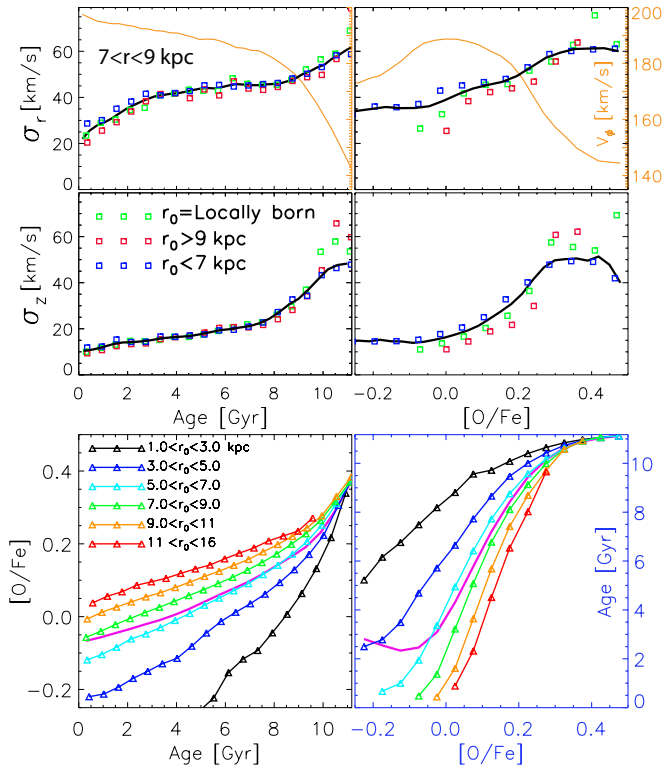


FIG. 6.— **Left column:** The age-velocity relations (AVR) resulting from our model in the radial (top panel) and vertical (middle panel) directions. The black solid lines show the AVR estimated from all stars in the annulus $7 < r < 9$ kpc. The green, red and blue squares plot the locally born stars, stars born in the outer disc ($r_0 > 9$ kpc), and in the inner disc ($r_0 < 7$ kpc), respectively. No significant contribution is found from samples arriving from different galactic radii. The bottom panel shows the relationship between age and $[\text{O}/\text{Fe}]$ for different birth-radius bins. **Right column:** The radial and vertical velocity dispersions as functions of $[\text{O}/\text{Fe}]$. The reason for the flattening at $[\text{O}/\text{Fe}] < -0.1$ is the mixture of stars of age < 4 Gyr. This can be seen easily in the bottom panel, which is similar to the one on the left, but with the horizontal and vertical axes reversed. The orange lines in the top row show the stellar rotational velocity, V_ϕ .

e.g., with the ongoing Gaia-ESO (Gilmore et al. 2012) or APOGEE (Majewski et al. 2010) surveys.

5.5. The age-Velocity and $[\text{O}/\text{Fe}]$ -Velocity relations

An important constraint in MW disc modeling is the observed velocity dispersion in the solar neighborhood. Due to the lack of good age estimates, the shape of the age-velocity relation (AVR) has been a matter of debate. While a power-law of the form $\sigma = t^{0.2-0.5}$ has been proposed (e.g., Wielen 1977; Dehnen and Binney 1998; Binney et al. 2000), some works have predicted an increase for stars younger than 2 Gyr, followed by a saturation up to ~ 10 Gyr, followed by a strong increase associated with the thick disc, possibly related to strong merger activity (or a single major merger) at high redshift (e.g., Freeman 1991; Edvardsson et al. 1993; Quillen and Garnett 2000).

In the left column, top two panels of Fig. 6 we present the radial and vertical velocity dispersions, σ_r and σ_z , as functions of age for stars in the simulated solar neighborhood ($7 < r < 9$ kpc). The solid black lines plot the total sample, while the differently color-coded squares show the locally born population (green), stars born in the outer disc (red) and stars born in the inner disc

(blue). Examining the total population, we note that for ages greater than ~ 3 Gyr, σ_r flattens significantly, rises only by 5 km/s in the time interval 3-8 Gyr, after which the slope increases again, finally reaching 60 km/s for the oldest stars. The σ_z behavior is somewhat different, with a smooth growth from 0 to 8 Gyr, followed by a steeper increase, even more drastic than σ_r , reaching about 50 km/s for the oldest stars. This is roughly consistent with the second scenario mentioned above. We must note, however, that some increase in velocity dispersion with age is always seen, except possibly in the range 6-8 Gyr for σ_r .

We now compare the contribution to the AVR from stars born in situ, inside the “solar” circle, and outside it. These three subpopulations, indicated by squares of different colors, show remarkably similar AVRs. The subsamples born outside/inside the radial bin considered have slightly lower/higher velocity dispersion as a function of age (except at the oldest ages, see below). This is consistent with the recent findings by Minchev et al. (2011b, 2012b), where it was demonstrated that migrators are generally not expected to heat the disc, due to the approximate conservation of the average radial and vertical actions in the absence of external perturbers. It is remarkable that we do not see any significant contribution here either, although the disc we study *is* perturbed by satellites, thus breaking the action invariance. We note that no massive mergers have occurred in our simulation for the last $\sim 8 - 9$ Gyr, which could explain this behavior. Interestingly, we find that, for the oldest population, the locally born stars have substantially higher velocity dispersions (especially σ_z) compared to the subsample coming from the inner disc (contrast green and blue squares for age $\gtrsim 10$ Gyr in the second row, left panel). This is in drastic contrast to the assumption made in a number of studies, that stars coming from the inner disc should heat vertically. The reason that, for the oldest population, the hottest stars were born in situ or outside the “solar” circle is related to the stronger effect of merger-induced perturbations in the outer disc (due to its exponential density decrease with radius), generally resulting in disc flaring (e.g., Bournaud et al. 2009). The larger σ_z -values for stars of age > 10 Gyr coming from the outer disc, compared to the locally born population, supports this conclusion (see also Sections 6.3 and 9.2).

Due to the lack of good age estimates, the $[\alpha\text{-elements}/\text{Fe}]$ ratios, such as $[\text{O}/\text{Fe}]$, are often used as proxies of age. To see how well age-velocity and $[\text{O}/\text{Fe}]$ -velocity relations match, in the top two panels of the right column of Fig. 6 we plot the radial and vertical velocity dispersions as functions of $[\text{O}/\text{Fe}]$. In agreement with the bottom right panel of Fig. 4, $[\text{O}/\text{Fe}]$ appears to follow age closely at the α -rich end, but not that well at low values. The stars born locally and outside the bin considered (green and red squares), show no information for $[\text{O}/\text{Fe}] \lesssim -0.07$ and $[\text{O}/\text{Fe}] \lesssim 0$, respectively. This can be related to our chemical evolution model (see the bottom left panel of Fig. 4).

What gives rise to the flattening at $[\text{O}/\text{Fe}] < -0.1$ seen for both σ_r and σ_z ? By inspecting the bottom panel of Fig. 5, we see that stars with $[\text{O}/\text{Fe}] < -0.1$ are born at $r_0 < 7$ kpc and have age $\lesssim 8$ Gyr, correlating inversely with birth radius. Therefore, the majority of stars with

$[\text{O}/\text{Fe}] < -0.1$ currently in the local bin, should have ages < 4 Gyr (see also bottom panel). Such a mixture of ages would naturally result in higher velocity dispersions. Indeed, the mean σ_r and σ_z for stars of age < 4 Gyr seen in the left column of Fig. 6, match well the corresponding, approximately constant, values at $[\text{O}/\text{Fe}] < -0.1$ in the right column.

Concentrating on the local population (green squares), we note markedly lower velocity dispersion values, compared to the total sample, at the lowest $[\text{O}/\text{Fe}]$ achieved. Inspecting the bottom panel of Fig. 5, it is evident that only the youngest locally born stars possess such low $[\text{O}/\text{Fe}]$, thus the velocity dispersions are similar to those of the youngest stars seen in the left panel. A similar argument explains the low σ_r and σ_z -values at $[\text{O}/\text{Fe}] \lesssim 0.1$ for stars originating in the outer disc (red squares). As in the plots on the left, for the high- $[\alpha/\text{Fe}]$ stars we find higher velocity dispersion values for locally born stars and inward migrators, compared to stars born in the inner disc. The reason for this was outlined above.

The orange curves in the top row of Fig. 6 show the stellar rotational velocity, V_ϕ , as a function of age (left) and $[\text{O}/\text{Fe}]$ (right). An inverse correlation between V_ϕ and σ_r is expected, due to the asymmetric drift effect. Naturally, a constant decrease in V_ϕ is seen with increasing age. Note that the oldest stars lag the younger population by ~ 50 km/s, similar to the rotational lag found for the thick-disc selection of clump giants by Soubiran et al. (2003), for example. The more complicated behavior found in the right panel is expected in view of our discussion above, where at low $[\text{O}/\text{Fe}]$ the population is a mixture of stars with ages up to ~ 4 Gyr. An upcoming paper is dedicated to the interpretation of the metallicity- V_ϕ relation.

5.6. The relation between age and $[\text{O}/\text{Fe}]$

We now briefly examine the relation between age and $[\text{O}/\text{Fe}]$ for stars ending up in our simulated solar vicinity. In the bottom left panel of Fig. 6 we plot $[\text{O}/\text{Fe}]$ as a function of age for six birth-radius bins at the final simulations time. The pink line shows the total sample, which, for age $\gtrsim 4$ Gyr, is seen to follow the stars with birth radii $5 < r_0 < 7$ kpc (cyan), rather than the locally born population (green). This goes well with Fig. 3, left panel, where it was seen that the r_0 -distribution peaks at around 6 kpc. For age $\lesssim 9$ Gyr, approximately linear relations are found for stars born in the same radial bins. However, due to contamination from radial migration, for the total sample the scatter increases strongly with decreasing age, in agreement with the bottom right panel of Fig. 4.

The bottom right panel of Fig. 6 shows age as a function of $[\text{O}/\text{Fe}]$. It is now easy to see the contribution from different galactic radii to the AVR in the panels above. As we found out earlier by different reasoning, stars at $[\text{O}/\text{Fe}] \lesssim -0.1$ are a mixture of ages < 4 Gyr. While following stars born at $r_0 \sim 6 - 8$ kpc (green and cyan bins) at age $\gtrsim 3.5$ Gyr, the total sample (pink line) shows an abrupt change for age < 3 Gyr, shifting toward the bin of birth radii $3 < r_0 < 5$ kpc. This introduces a strong non-linearity in the age- $[\text{O}/\text{Fe}]$ relation for these younger ages.

In summary, the approximately linear relation between age and $[\text{O}/\text{Fe}]$ for stars born at the same radius is de-

stroyed when radial migration is taken into account. When grouped by common birth radii, each sample is a quite good age-indicator, in the covered $[\text{O}/\text{Fe}]$ region, e.g., in the range $-0.1 \lesssim [\text{O}/\text{Fe}] \lesssim 0.4$ for the locally born stars. However, due to the inevitable radial mixing, the overlap of these sub-populations, combined with the offset in the $[\text{O}/\text{Fe}]$ -range covered, contaminate this relation.

5.7. The vertical structure of the local disc

We now study the density and vertical velocity as functions of height above the disc plane in the annulus $7 < r < 9$ kpc. Unlike the common division into thin and thick discs, we chose to divide our sample in groups by age, $[\text{O}/\text{Fe}]$, or $[\text{Fe}/\text{H}]$.

In the first row of Fig. 7 we show the vertical velocity dispersion as a function of height above the disc plane, $\sigma_z(z)$, for stars in the “solar” vicinity ($7 < r < 9$ kpc) binned in six different groups by age (triangles, left), $[\text{O}/\text{Fe}]$ (squares, middle), and $[\text{Fe}/\text{H}]$ (squares, right). The corresponding bin values are shown to the right of the figure. Very similar increasing trends are seen for young stars, low- $[\alpha/\text{Fe}]$ and metal-rich bins ($\sigma_z \sim 10 - 20$ kpc). Interestingly, as populations get older, relations flatten around ~ 50 km/s for the oldest/high- $[\alpha/\text{Fe}]$ /metal-poor samples. Both these trends and values are similar to the recent observational results by Bovy et al. (2012c). We note that in our work subpopulations are in narrow bins of $[\text{O}/\text{Fe}]$ or $[\text{Fe}/\text{H}]$, but not both at the same time, as done by Bovy et al. (2012c). Nevertheless, the similarity with their Fig. 2, bottom, is obvious.

The second row of Fig. 7 displays the vertical disc scale-height at the “solar” radius binned in the same groups as in the first row. We find that single exponentials can fit reasonably well each subsample, as well as the total population. The color-coded values, h , indicate single exponential fits, over-plotted by the dotted lines (dashed black line for the total population). No smoothing is applied. Gradual trends are seen for all panels, where values of h grow with increasing age, increasing $[\text{O}/\text{Fe}]$, and decreasing $[\text{Fe}/\text{H}]$.

Older samples are always expected to have higher velocity dispersion, on the average, than younger ones, due to their being exposed longer to a variety of heating agents. As older samples are high- $[\alpha/\text{Fe}]$ and metal-poor, the trends seen with mean height above the disc plane are not surprising. It is not necessarily obvious why single exponential would provide good fits to stars in narrow abundance or age bins. As we show in Paper II, this is not expected throughout the entire disc extent.

The variation of scale-height for different subpopulations, as well as the fact that we can fit single exponentials to them, are consistent with the findings of Bovy et al. (2012a), based on G-type SEGUE dwarf data. Again, we point out that we have constrained samples either by $[\text{O}/\text{Fe}]$ or $[\text{Fe}/\text{H}]$, but not both, as Bovy et al. did.

It is also interesting to consider the variation of $[\text{Fe}/\text{H}]$ with height above the disc plane, z , as well as with mean vertical velocity, v_z . In Fig. 8 we show these trends for the same bins of age (left) and $[\text{O}/\text{Fe}]$ (right) used for Fig. 7. The solid black lines in each panel display the total number of stars in the annulus $7 < r < 9$ kpc. We

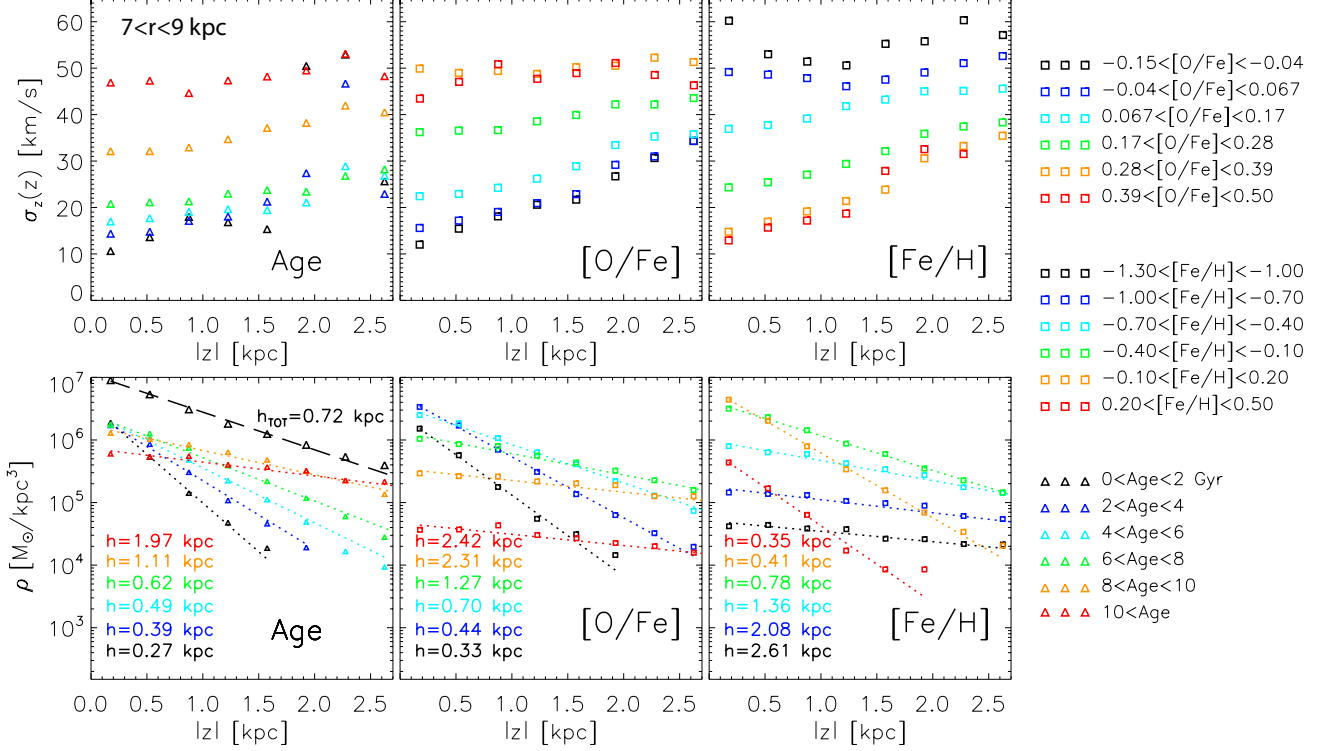


FIG. 7.— **First row:** The vertical velocity dispersion as a function of height above the disc plane, $\sigma_z(z)$, for stars in the “solar” vicinity binned in six different groups by age (left), $[\text{O}/\text{Fe}]$ (middle), and $[\text{Fe}/\text{H}]$ (right). The corresponding bin values are shown to the right of the figure. Very similar increasing trends are seen for young stars, α -poor and metal-rich bins ($\sigma_z \sim 10 - 20$ kpc). As populations get older, relations flatten. **Second row:** Same as above, but for the vertical scale-heights. The color-coded values, h , indicate single exponential fits, shown by the dotted lines (dashed black line for the total population). Smooth increase of scale-height is seen with increasing age, increasing $[\text{O}/\text{Fe}]$, and decreasing $[\text{Fe}/\text{H}]$.

consider stars above and below the plane and take the mean absolute values $|z|$ and $|v_z|$. A negative trend is seen for both $|z|$ and $|v_z|$ as expected from observations (e.g., Katz et al. 2011; Schlesinger et al. 2011).

When divided into age or $[\text{O}/\text{Fe}]$ subsamples, the variation of $[\text{Fe}/\text{H}]$ is mostly lost for each individual group. This is true for both $|z|$ and $|v_z|$. It is then clear, that the downtrend in the total sample comes from the fact that younger (or α -young) stars are, on the average, both metal-rich and more numerous at small distances from the plane. With increasing height the density of older (large $[\text{O}/\text{Fe}]$ -ratios), and thus more metal-poor, populations continuously increases, resulting in the overall negative gradient.

Similarly, younger stars are confined close to the disc and, thus, have relatively low vertical velocities. With increasing age (and thus velocity dispersion) the amplitude of vertical oscillations increases, while the stellar density decreases. This, again, results in the negative trend of $[\text{Fe}/\text{H}]$. The flattening at $|v_z| \gtrsim 90$ km/s is due to the fact that the number of stars with such high velocities is almost exclusively dominated by the oldest/ $[\text{O}/\text{Fe}]$ -rich stars.

The approximately flat mean $|z|$ - $[\text{Fe}/\text{H}]$ and $|v_z|$ - $[\text{Fe}/\text{H}]$ relations for stars of narrow age- or $[\text{O}/\text{Fe}]$ -bins is an extension to the similar behavior seen in the $|z| - \sigma_{z,r}$ plots above and provides additional predictions for Galactic surveys.

6. RELATION TO RECENT OBSERVATIONAL RESULTS

We have already shown that a number of the basic observed chemistry and kinematics of solar neighborhood

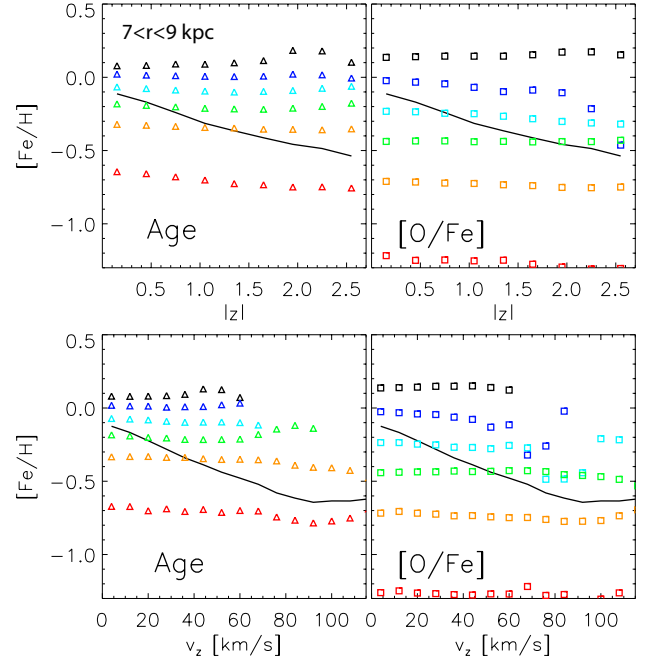


FIG. 8.— **First row:** $[\text{Fe}/\text{H}]$ as a function of height above the disc plane (absolute value), $|z|$, for stars in the “solar” vicinity. Different colors indicate age (left) or $[\text{O}/\text{Fe}]$ (right) for the same bins as in Fig. 4. **Second row:** Same as above but the vertical axes show the absolute mean vertical velocity, $|v_z|$. The solid black curve in each panel shows the relation for the total sample.

stars can be explained by our model. We now perform some further tests, accounting roughly for sample biases

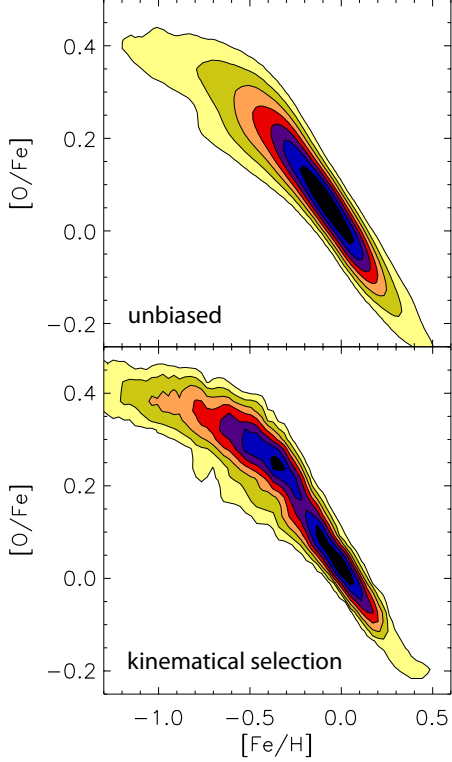


FIG. 9.— Selection effects can result in a bimodality in the $[\text{Fe}/\text{H}]$ - $[\text{O}/\text{Fe}]$ plane. The top panel shows the unbiased stellar density distribution, as in Fig. 4. In the bottom plot we have applied the selection criteria used by Bensby et al. (2003).

encountered in different surveys.

6.1. Is the bimodality in the $[\text{Fe}/\text{H}]$ - $[\text{O}/\text{Fe}]$ plane due to selection effects?

Starting with the assumption of two distinct entities – the thin and thick discs – many surveys select stars according to certain kinematical criteria (e.g., Bensby et al. 2003; Reddy et al. 2006). For example, Bensby et al. (2003) defined a (now widely used) method for preferentially selecting thin- and thick-disc stars with a probability function purely based on kinematics.

Starting with the smooth $[\text{Fe}/\text{H}]$ - $[\text{O}/\text{Fe}]$ stellar density distribution, presented in Fig. 4, we now employ the same technique as Bensby et al. (2003) and extract a thin- and thick-disc selections from our initially unbiased sample. In order to obtain a similar number of thin- and thick-disc stars, as done in most surveys, we randomly down-sample the thin-disc selection.

The results are presented in Fig. 9, where the top panel shows the unbiased distribution. In the bottom panel we have applied the selection criteria as described above. We find a discontinuity at $[\text{O}/\text{Fe}] \approx 0.15-0.2$, similarly to what is seen in a number of observational studies. This test shows that selecting stars kinematically can give preference to the two extremes of the distribution (oldest vs youngest), resulting in the gap we find.

6.2. Changes in the MDF for samples at different distances from the disc plane

To be able to compare our results to different MW surveys we need to constrain spatially our sample. For example the GCS stellar sample is confined to within

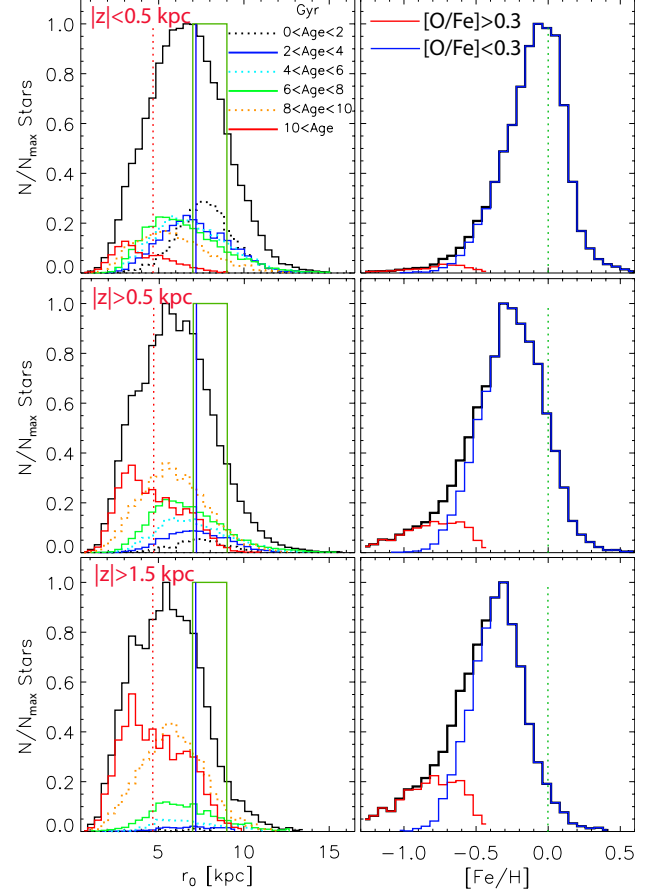


FIG. 10.— Changes in the metallicity distribution function (MDF) for samples at different distances from the disc plane. **First column:** Distribution of birth radii for stars ending up in the bin $7 < r < 9$ kpc (green rectangle) at the final time. The bar CR and OLR are indicated by the dotted red and solid blue vertical lines. From top to bottom, we have applied the selection criteria $|z| < 0.5$, $|z| > 0.5$, and $|z| > 1.5$ kpc. **Second column:** MDF for the same particle subsets as on the left. The black line shows the total population for each selection, while the red and blue colors indicate $[\text{O}/\text{Fe}] > 0.3$ and $[\text{O}/\text{Fe}] < 0.3$, respectively. A shift in the peak from $[\text{Fe}/\text{H}] = 0$ to negative values is seen with increasing distance from the disc plane.

100 pc from the Sun, while the SEGUE and RAVE samples explore much larger regions, but miss the local stars. To see the biases introduced in the MDF when distance cuts are applied, we explore three possibilities.

Figure 10 shows our predicted metallicity distribution function at the solar vicinity, for different heights from the plane. From top to bottom, we have applied the selection criteria $|z| < 0.5$ (which is similar to what is seen by GCS), $|z| > 0.5$, and $|z| > 1.5$ kpc (similar to what is seen in SEGUE by Schlesinger et al. 2011). The left column shows the distribution of birth radii for stars ending up in the bin $7 < r < 9$ kpc (green rectangle) at the final time, whereas the right column shows the metallicity distribution for the same particle subsets as on the left. In the right column the black line shows the total population for each selection, while the red and blue colors indicate $[\text{O}/\text{Fe}] > 0.3$ and $[\text{O}/\text{Fe}] < 0.3$, respectively. It can be seen that the MDF peak shifts from solar at low heights from the plane (consistent with the GCS sample, e.g., Casagrande et al. 2011), to a value below solar, as we select only particles with heights above 500 pc (con-

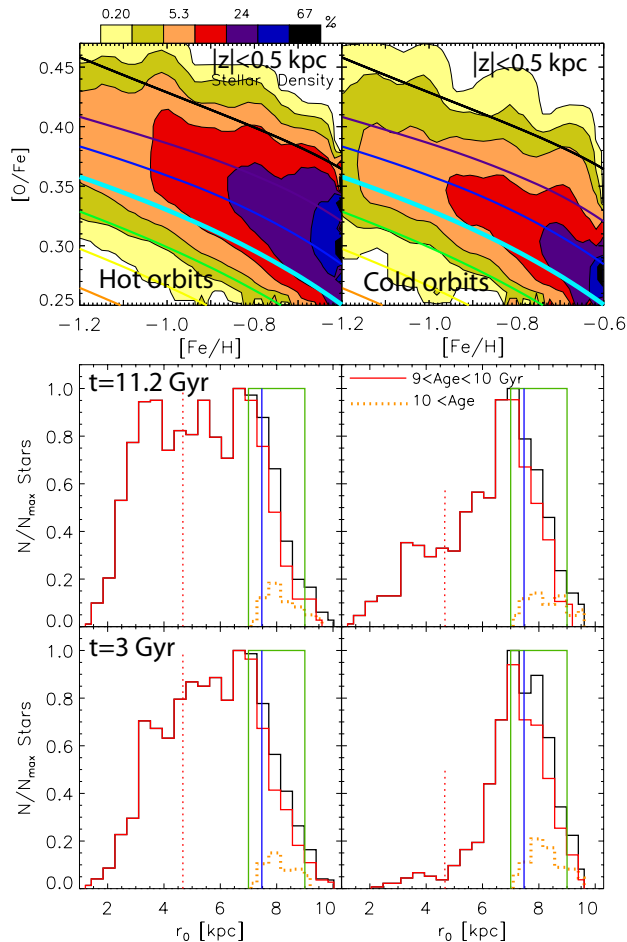


FIG. 11.— **First row:** $[\text{Fe}/\text{H}]-[\text{O}/\text{Fe}]$ stellar density distributions for metal-poor, high- $[\text{O}/\text{Fe}]$ stars ending up in the cylinder $7 < r < 9$ kpc, $0.5 < |z| < 2.5$ kpc. Stars are separated into a “cold” and “hot” samples with corresponding velocity dispersions $\sigma_r \approx 65$ and $\sigma_r \approx 28$ km/s. **Second row:** Birth radii distributions for two age groups, as indicated. **Third row:** Same as the second row, but at $t = 3$ Gyr, i.e., 0.5 Gyr after the most massive merger has concluded. A large fraction of stars for both the hot and cold samples are in place at that time.

sistent with RAVE – Boeche et al. 2012, In prep. and SEGUE – Schlesinger et al. 2011). In the latter case a value of $[\text{Fe}/\text{H}] \sim -0.3$ is found, strikingly similar to the one found by Schlesinger et al. (2011). Note that even at large distance from the plane, the MDF is dominated mostly by stars with $[\text{O}/\text{Fe}] < 0.3$, whereas the higher $[\text{O}/\text{Fe}]$ values are always contributing to its metal-poor tail. This suggests a bias in the distributions obtained by Lee et al. (2011), as discussed by Bovy et al. (2012a,b,c).

6.3. The origin of stars with low-metallicity and high- $[\text{O}/\text{Fe}]$ ratios

Analyzing the SEGUE G-dwarf data, Liu and van de Ven (2012) argued that (internally driven) radial migration cannot be responsible for the origin of the hot, metal-poor, high- $[\text{O}/\text{Fe}]$ stars and proposed that they have formed through early-on gas-rich mergers.

We now search for the origin of the metal-poor high- $[\text{O}/\text{Fe}]$ stars in our simulation. To approximate the spatial coverage of the SEGUE G-dwarf sample, we consider stars in the annulus $7 < r < 9$ kpc and distance from the

plane $0.5 < |z| < 2.5$ kpc. As in Liu and van de Ven (2012) (their group III) we consider stars with $-1.2 < [\text{Fe}/\text{H}] < -0.6$ and $0.25 < [\text{O}/\text{Fe}] < 0.47$. Finally, we apply a cut in eccentricities at $e = 0.2$, thus separating our sample into a “cold”¹⁴ and “hot” subgroups with corresponding radial velocity dispersions $\sigma_r \sim 27$ and 67 km/s. The ratio of cold to hot orbits is ~ 0.3 .

In the top row of Fig. 11 we plot stellar density contours of the $[\text{Fe}/\text{H}]-[\text{O}/\text{Fe}]$ relation for the hot (left) and cold (right) orbits. As in Fig. 4, we overlay the input chemistry for different initial radii, where the thick cyan curve corresponds to $r = 8$ kpc and the rest are separated by two kpc (black for $r = 2$ kpc). We can already see that a large number of stars come from the inner disc, especially for the hot sample.

The second row shows that initial radii span the range $1 < r_0 < 10$ kpc for both samples, but the distribution for the cold orbits is heavier near the solar vicinity. The majority of stars have age > 10 Gyr (solid red line) with initial radii spread all over the disc. A much smaller group of stars with $9 < \text{age} < 10$ Gyr (dotted orange) originates at the solar vicinity. The r_0 -distribution of stars older than ~ 10 Gyr is an example of extremely efficient migration, usually not seen as the effect of internal perturbations.

To get an idea of when these stars arrive to the solar neighborhood, in the third row of Fig. 11 we plot the distribution of initial radii obtained 3 Gyr after the beginning of disc formation. At this early stage we already see distributions similar to the ones we find “today”. For example, there are three peaks in the r_0 -distribution at $\approx 3.5, 5$, and 7 kpc for both hot samples and the cold selection today. Note that not all of the stars found in the solar vicinity at $t = 3$ Gyr would remain there for the next ~ 8 Gyr due to the continuous migration. Additionally, part of the cold sample at $t = 3$ Gyr would heat up, ending up in the hot one we see today.

What causes the extreme migration at $t < 3$ Gyr? As mentioned in Sec. 2, the last massive merger (1:5 mass ratio) begins at $t \approx 1.5$ and is disrupted by $t \approx 2.5$ Gyr, or just before the $t = 3$ Gyr distributions shown in Fig. 11. The strong effect on the changes of stellar angular momenta around this time were presented in Fig. 1, bottom left panel, leaving no doubt that this event is responsible for the vehement migration we find. In the Appendix (Sec. 9.3, Fig. 14) we demonstrate that the merger-induced migration suppresses heating both in the vertical and radial directions. On the contrary, after the merger has concluded, the already *preheated* inner disc is a source of hot stars, thus contributing to disc heating via migration induced by the bar and spirals. As the disc grows further from gas accretion, this effect becomes much smaller.

Further contribution from the bar in migrating old stars out is expected at $t > 3$ Gyr, as inferred from the increase in the r_0 -distributions at ~ 3.5 kpc at the final time (middle row). It should be kept in mind that migration efficiency decreases with increasing velocity dispersion (e.g., Comparella and Quillen 2012), presenting an extreme case in the current kinematic selection.

¹⁴ Here we are somewhat stretching the meaning of “cold” orbits. Usually, for stars at the solar radius, this would be a sample with $\sigma_r \sim 5 - 10$ km/s.

Therefore, the bar and spirals at later times would be mostly transferring cold orbits, populating the region at $r_0 \lesssim 6.5$ kpc in the cold distribution.

Liu and van de Ven (2012) argued that the old, hot, metal-poor, high-[O/Fe] stars were born hot in gas-rich mergers. Our analysis above suggests a very similar interpretation (although our disc does not experience a large number of gas-rich mergers), in the sense that stars were born hot and further heated by mergers, which also gives rise to large-scale, very efficient migration. We also find, however, that further migration at later times, driven by the bar and spirals, is essential, as discussed above.

To see when the oldest stars migrate to the solar neighborhood in the lack of early massive mergers, we performed a different model realization for which the dynamics is quiescent and migration is driven mostly by internal perturbers (Appendix, Sec. 9.1). We show in the Appendix (Sec. 9.2, Fig. 13) that a sizable fraction of metal-poor, high-[O/Fe] stars can, nevertheless, migrate to the solar neighborhood as the effect of the bar. However, this happens over the entire evolution of the disc and the ratio of cold to hot number of objects is now ~ 0.9 (to be compared to 0.3 in our stander model), related to the overall low final velocity dispersions. In a properly mass-corrected observational data this ratio can be used as a discriminant for the two type of scenarios. A possible deficiency in the no-merger case is that velocity dispersion for the oldest stars is underestimated by a factor of ~ 2 . This is consistent with the results by Minchev et al. (2012b), in showing that internally driven migration does not contribute to disc heating.

7. A UNIFYING MODEL FOR THE MILKY WAY THICK DISC

We now focus our attention on the properties of the oldest stars ($\text{age} \gtrsim 10$ Gyr) in our model. This subsample is marked by

- a metallicity distribution which peaks at $[\text{Fe}/\text{H}] \sim -0.5$ and has a metal-poor tail down to $[\text{Fe}/\text{H}] \sim -1.3$ (Fig. 4, upper right panel).
- [O/Fe]-values spanning the range $0.2 - 0.4$, with a peak around 0.3 (Fig 4, lower right panel).
- a lag in the rotational velocity by ~ 50 km/s compared to the young stars (Fig. 6, top row).
- large velocity dispersions (Fig. 6).
- a large scale-height (Fig. 7, bottom row).

All of these properties are strikingly reminiscent of what we call the “thick disc” of our Galaxy, despite the fact that we have used pure thin-disc chemistry. Within the frameworks of the model we present here, the MW thick disc has emerged from (i) stars born hot and heated by mergers at early times and (ii) radial migration (from mergers at early times and bar/spirals later on) transporting these old stars from the inner disc to the solar vicinity.

Such a conclusion is in agreement with most (seemingly contradicting) models of thick-disc formation, which expect contribution from only/mostly one of the following: (i) mergers, (ii) early formation in gas-rich, turbulent clumpy discs, or gas rich mergers, and (iii) radial

migration driven by internal instabilities. A combination of these mechanisms working together is required, where strong heating and migration occurs early on from external perturbations (our case) and/or turbulent gas clumps, followed by radial migration taking over the disc dynamics at later times. Yes, mergers are important, but we also need radial migration (unavoidable if a bar, spiral structure and/or mergers are present) to transport out old, hot stars, with thick-disc chemical characteristics. Yes, migration is important, but the old stars need to be “preheated” by being born hot and/or were heated by mergers at high redshift (also unavoidable from our current understanding of cosmology).

The high stellar birth velocity dispersions at high redshift we find in our simulation (~ 50 km/s) is consistent with recent works (Forbes et al. 2012; Brook et al. 2012). An important dynamical consequence of this is that the disc becomes less susceptible to satellite perturbations (common at high redshift), making it easier to survive until today.

Radial gradients for different height above the disc plane, as well as the scale-length of this “thick disc” population will be discussed in detail in Paper II.

8. CONCLUSIONS

In this work we presented a new approach for studying the chemodynamical evolution of galactic discs, with special emphasis on the Milky Way (MW). Unlike other similar studies, where either the dynamics is too simplistic or the star formation history (SFH) and chemistry enrichment are unconstrained, our chemodynamical model is a fusion between a pure chemical evolution model and a high-resolution simulation in the cosmological context. As we argued in Sec. 4, this new approach allows us to bypass most known problems encountered in self-consistent simulations, where chemical enrichment still proves to be a challenge (see Sec. 1.2). Moreover, this is the first time that a chemodynamical model has the extra constraint of defining a realistic solar vicinity also in terms of dynamics (see Sec. 2).

The main results of our chemodynamical model can be summarized as follows:

- The distribution of birth radii, r_0 , of stars ending up in a solar neighborhood-like location after 11.2 Gyr of evolution peaks close to $r_0 = 6$ kpc due to radial migration (left panel of Fig. 3). The strongest effect from radial migration is found for the oldest stars, related to the 1:5 mass-ratio merger in our simulation ~ 9 Gyr ago. Locally born stars of all ages can be found in the solar neighborhood. While a wide range of birth radii is seen for different age groups, the majority of the youngest stars are born at, or close to, the solar neighborhood bin.

- While the low-end in our simulated metallicity distribution is composed by stars with a wide range of birth radii, the tail at larger metallicities ($0.25 < [\text{Fe}/\text{H}] < 0.6$) results almost exclusively from stars with $3 < r_0 < 5$ kpc. This is the region just inside the bar’s CR, which is where the strongest outward radial migration occurs, as we discussed in Sec. 2 and showed in the bottom row of Fig. 1. The fraction of stars in this tail can, therefore, be related to the bar’s dynamical properties, such as its strength, pattern speed and time evolution/formation.

- Our results suggest that the most likely birth location

for the Sun is in the range $4.4 < r_0 < 7.7$ kpc, with the highest probability ~ 5.6 kpc, followed by ~ 7 kpc (Fig. 3, right). This estimate comes from both dynamical and chemical constraints and is dependent on the migration efficiency in our simulation and the adopted chemical evolution model.

- Examining the effect on the age-metallicity relation (AMR), we find that some flattening is observed, mostly for ages $\gtrsim 5$ Gyr (Fig. 4). Although significant radial mixing is present, a slope in the AMR is preserved, with a scatter compatible with recent observational work.

- We find no bimodality in the $[\text{Fe}/\text{H}]-[\text{O}/\text{Fe}]$ stellar density distribution. However, when selecting particles according to kinematical criteria used in high-resolution samples to define thin and thick discs, we recover the observed discontinuity in the $[\text{O}/\text{Fe}]-[\text{Fe}/\text{H}]$ plane (Fig. 9). This is in agreement with the recent observational results by Bovy et al. (2012b), where a smooth $[\text{Fe}/\text{H}]-[\text{O}/\text{Fe}]$ distribution was obtained, after correcting for the spectroscopic sampling of stellar sub-populations in the SEGUE survey.

- By separating our simulated local sample into narrow bins of age, $[\text{O}/\text{Fe}]$, and $[\text{Fe}/\text{H}]$, we found that the vertical scale-height of each component can be fitted well by a single exponential, with values growing with increasing age, increasing $[\text{O}/\text{Fe}]$, and decreasing metallicity (Fig. 7, bottom). The vertical velocity dispersions for each of these subpopulation was found to exhibit smooth variations with height above the disc plane, strongly flattening for old, high- $[\text{O}/\text{Fe}]$, and metal-poor stars. Our model reproduces qualitatively (and in many cases quantitatively) the observational results by Bovy et al. (2012a,c).

- We predict approximately flat $|z|-[Fe/H]$ and $|v_z|-[Fe/H]$ (perhaps anticipated) relations for stars of narrow age- or $[\text{O}/\text{Fe}]$ -bins (Fig. 8). This is an extension to the similar behavior seen in the $|z| - \sigma_{z,r}$ plots above and provides additional predictions for Galactic surveys.

- The local age-velocity relation (AVR) in the radial direction, σ_r , resulting from our model plateaus for stars of age 3-8 Gyr, while a weak increase is found for the vertical component, σ_z (Fig. 6). For ages greater than 8 Gyr, a continuous increase is observed for both components, related to the massive merger in our simulation ~ 9 Gyr ago. These hot stars can be associated with a thick disc. In contrast, internally driven migration does not result in high enough velocity dispersions for the old stars (see Sec. 9.1, Fig. 12).

- We found a strong flattening in the $[\text{Fe}/\text{H}]$ radial profiles of the older populations, however, the younger ones are much less affected (see Fig. 5). Remarkably, for stars younger than 2 Gyr the final gradient is very similar to the initial one out to ~ 12 kpc, justifying its use as a constraint for our chemical model.

- We predict that the $[\text{O}/\text{Fe}]$ radial profiles are essentially preserved for the chemical model we use. The $[\text{O}/\text{Fe}]$ profiles for different age groups result straightforwardly from the adopted variation of the infall-law with radius (and hence the SFHs at different positions) and, thus, provide a way to constrain different chemical evolution models. In the near future, these would be possible to measure by combining the good distances and ages expected from the CoRoT mission (Baglin et al. 2006), with abundance ratios obtained by spectroscopic follow-up surveys. For the young populations, this should be al-

ready possible to be obtained from the observations of open clusters, e.g., with the ongoing Gaia-ESO or APOGEE surveys.

- Finally, probably one of the most important outcomes of our chemodynamical model is that, although we used only a thin-disc chemical evolution model, the oldest stars that are now in the solar vicinity show several of the properties usually attributed to the Galactic thick disc. In other words, according to the results of the present work, the MW “thick disc” emerges naturally from stars migrating from the inner disc very early on due to strong merger activity in the first couple of Gyr of disc formation, followed by further radial migration driven by the bar and spirals at later times (see Sec. 6.3).

We showed that hot, old, metal-poor, high- $[\alpha/\text{Fe}]$ stars can be delivered to the solar neighborhood at high redshift as the effect of a massive perturber (1:5 mass ratio in our simulation, see Fig. 11). For a MW-size galaxy, a merger of this size around $z \sim 1$ is consistent with the numerical results by a number of groups (e.g., Benson et al. 2004; Stoehr 2006; Kazantzidis et al. 2008; De Lucia and Helmi 2008; Stewart et al. 2008; Villalobos and Helmi 2008; Purcell et al. 2009).

Alternatively, a bar can also bring some fraction of these stars to the solar neighborhood, but over a large period of time, as we showed in Sec. 9.2 in the Appendix. However, a difference in the metallicity and velocity distributions of these old stars would result. Most notably, avoiding a merger not only avoids the extreme migration at high redshift, but also does not result in high enough velocity dispersions today. For example, we find AVRs with maxima at $\sigma_r \approx 43$ km/s and $\sigma_z \approx 25$ km/s in the lack of strong mergers (to be compared to ≈ 60 and ≈ 50 km/s, respectively). Additionally, the ratio of cold to hot orbits changes from ~ 0.3 to ~ 0.9 when the merger is avoided. This larger difference can be used as a constraint in properly mass-corrected observational data to assess the possibility of an early-on merger in the MW.

It is, therefore, tempting to conclude that stars with thick-disc chemistry and kinematics have migrated to the solar vicinity early on as the result of a sufficiently massive merger. For an efficient migration, we should expect a merger on a radial orbit (Quillen et al. 2009) penetrating deep into the disc. Equivalently, it may be possible that a series of sufficiently massive minor mergers (e.g., 1:10 mass ratio) acting over a short time period ($\sim 1 - 2$ Gyr) may give a similar result.

The bar in our simulations has a size at the final time, similar to the one seen in the MW, however, it is quite weak before the last $\sim 5-6$ Gyr of evolution and it does not show buckling, although the bulge appears boxy. It may be that our Galaxy hosted a stronger bar than the one we consider here, which would result in an even stronger migration from the inner disc. It would be interesting to explore disc models with different bar sizes, as well as cases where a strong buckling instability takes place.

While here we concentrated on the solar vicinity, results for the entire disc will be presented in Paper II of this series. Chemodynamical predictions for different disc radii may help further constraints thick-disc formation scenarios and the MW assembly in general.

The novel method presented here is potentially very useful and easy to implement. A suite of different chem-

ical evolution models assigned to different disc dynamics (from different simulations) should be investigated to make progress in the field of Galactic Archeology.

REFERENCES

- Abadi, M. G., Navarro, J. F., Steinmetz, M., and Eke, V. R.: 2003, *ApJ* **597**, 21
- Agertz, O., Teyssier, R., and Moore, B.: 2011, *MNRAS* **410**, 1391
- Allende Prieto, C., Majewski, S. R., Schiavon, R., Cunha, K., Frinchaboy, P., Holtzman, J., Johnston, K., Shetrone, M., Skrutskie, M., Smith, V., and Wilson, J.: 2008, *Astronomische Nachrichten* **329**, 1018
- Asplund, M., Grevesse, N., Sauval, A. J., and Scott, P.: 2009, *ARA&A* **47**, 481
- Babusiaux, C. and Gilmore, G.: 2005, *MNRAS* **358**, 1309
- Baglin, A., Auvergne, M., Barge, P., Deleuil, M., Catala, C., Michel, E., Weiss, W., and COROT Team: 2006, in M. Fridlund, A. Baglin, J. Lochard, and L. Conroy (eds.), *ESA Special Publication*, Vol. 1306 of *ESA Special Publication*, p. 33
- Bensby, T., Feltzing, S., and Lundström, I.: 2003, *A&A* **410**, 527
- Benson, A. J., Lacey, C. G., Frenk, C. S., Baugh, C. M., and Cole, S.: 2004, *MNRAS* **351**, 1215
- Binney, J., Dehnen, W., and Bertelli, G.: 2000, *MNRAS* **318**, 658
- Binney, J., Gerhard, O., and Spergel, D.: 1997, *MNRAS* **288**, 365
- Binney, J. and Tremaine, S.: 2008, *Galactic Dynamics: Second Edition*, Princeton University Press
- Bird, J. C., Kazantzidis, S., and Weinberg, D. H.: 2012, *MNRAS* **420**, 913
- Bonanno, A., Schlattl, H., and Paternò, L.: 2002, *A&A* **390**, 1115
- Bournaud, F. and Combes, F.: 2002, *A&A* **392**, 83
- Bournaud, F., Elmegreen, B. G., and Martig, M.: 2009, *ApJ* **707**, L1
- Bovy, J., Rix, H.-W., and Hogg, D. W.: 2012a, *ApJ* **751**, 131
- Bovy, J., Rix, H.-W., Hogg, D. W., Beers, T. C., Lee, Y. S., and Zhang, L.: 2012b, *arXiv:1202.2819*
- Bovy, J., Rix, H.-W., Liu, C., Hogg, D. W., Beers, T. C., and Lee, Y. S.: 2012c, *ApJ* **753**, 148
- Brook, C. B., Gibson, B. K., Martel, H., and Kawata, D.: 2005, *ApJ* **630**, 298
- Brook, C. B., Kawata, D., Gibson, B. K., and Freeman, K. C.: 2004, *ApJ* **612**, 894
- Brook, C. B., Stinson, G. S., Gibson, B. K., Kawata, D., House, E. L., Miranda, M. S., Macciò, A. V., Pilkington, K., Roškar, R., Wadsley, J., and Quinn, T. R.: 2012, *arXiv:1206.0740*
- Brunetti, M., Chiappini, C., and Pfenniger, D.: 2011, *A&A* **534**, A75
- Calura, F., Gibson, B. K., Michel-Dansac, L., Stinson, G. S., Pilkington, K., House, E. L., Brook, C. B., Few, C. G., Bailin, J., Couchman, H. M. P., Wadsley, J., and .: 2012, *arXiv:1204.1051*
- Casagrande, L., Schönrich, R., Asplund, M., Cassisi, S., Ramírez, I., Meléndez, J., Bensby, T., and Feltzing, S.: 2011, *A&A* **530**, A138
- Castro, S., Rich, R. M., Grenon, M., Barbuy, B., and McCarthy, J. K.: 1997, *AJ* **114**, 376
- Chiappini, C.: 2009, in J. Andersen, J. Bland-Hawthorn, & B. Nordström (ed.), *IAU Symposium*, Vol. 254 of *IAU Symposium*, pp 191–196
- Chiappini, C.: 2012, *Red Giant Stars: Probing the Milky Way Chemical Enrichment*, p. 147
- Chiappini, C., Górný, S. K., Stasińska, G., and Barbuy, B.: 2009, *A&A* **494**, 591
- Chiappini, C., Matteucci, F., and Gratton, R.: 1997, *ApJ* **477**, 765
- Chiappini, C., Matteucci, F., and Romano, D.: 2001, *ApJ* **554**, 1044
- Chiappini, C., Romano, D., and Matteucci, F.: 2003, *MNRAS* **339**, 63
- Christensen-Dalsgaard, J.: 2009, in E. E. Mamajek, D. R. Soderblom, and R. F. G. Wyse (eds.), *IAU Symposium*, Vol. 258 of *IAU Symposium*, pp 431–442
- Comparella, J. and Quillen, A. C.: 2012, *arXiv:1207.5753*
- Contopoulos, G. and Papayannopoulos, T.: 1980, *A&A* **92**, 33
- de Jong, R. S., Bellido-Tirado, O., and Chiappini, C. e. a.: 2012, *arXiv:1206.6885*
- De Lucia, G. and Helmi, A.: 2008, *MNRAS* **391**, 14
- Dehnen, W.: 2000, *AJ* **119**, 800
- Dehnen, W. and Binney, J. J.: 1998, *MNRAS* **298**, 387
- Di Matteo, P., Lehnert, M. D., Qu, Y., and van Driel, W.: 2011, *A&A* **525**, L3
- Drimmel, R. and Spergel, D. N.: 2001, *ApJ* **556**, 181
- Edvardsson, B., Andersen, J., Gustafsson, B., Lambert, D. L., Nissen, P. E., and Tomkin, J.: 1993, *A&A* **275**, 101
- Ellison, S. L., Nair, P., Patton, D. R., Scudder, J. M., Mendel, J. T., and Simard, L.: 2011, *MNRAS* **416**, 2182
- Few, C. G., Courty, S., Gibson, B. K., Kawata, D., Calura, F., and Teyssier, R.: 2012, *MNRAS* **424**, L11
- Forbes, J., Krumholz, M., and Burkert, A.: 2012, *ApJ* **754**, 48
- Freeman, K.: 2012, *Structure and Evolution of the Milky Way*, p. 137
- Freeman, K., Bland-Hawthorn, J., and Barden, S.: 2010, *AAO Newsletter* (February), in press
- Freeman, K. C.: 1991, in B. Sundelius (ed.), *Dynamics of Disc Galaxies*, pp 15–
- Fuhrmann, K.: 1998, *A&A* **338**, 161
- Fuhrmann, K.: 2008, *MNRAS* **384**, 173
- Gerhard, O.: 2011, *Memorie della Societa Astronomica Italiana Supplementi* **18**, 185
- Gerhard, O. E.: 2001, in J. G. Funes and E. M. Corsini (eds.), *Galaxy Disks and Disk Galaxies*, Vol. 230 of *Astronomical Society of the Pacific Conference Series*, pp 21–30
- Gilmore, G., Randich, S., Asplund, M., Binney, J., Bonifacio, P., Drew, J., Feltzing, S., Ferguson, A., Jeffries, R., Micela, G., Negueruela, I., Prusti, T., Rix, H.-W., Vallenari, A., Alfaro, E., Allende-Prieto, C., Babusiaux, C., Bensby, T., Blomme, R., Bragaglia, A., Flaccomio, E., François, P., Irwin, M., Koposov, S., Korn, A., Lanzafame, A., Pancino, E., Paunzen, E., Recio-Blanco, A., Sacco, G., Smiljanic, R., Van Eck, S., and Walton, N.: 2012, *The Messenger* **147**, 25
- Gómez, F. A., Minchev, I., O’Shea, B. W., Beers, T. C., Bullock, J. S., and Purcell, C. W.: 2012a, *arXiv:1207.3083*
- Gómez, F. A., Minchev, I., O’Shea, B. W., Lee, Y. S., Beers, T. C., An, D., Bullock, J. S., Purcell, C. W., and Villalobos, Á.: 2012b, *MNRAS* **423**, 3727
- Gómez, F. A., Minchev, I., Villalobos, Á., O’Shea, B. W., and Williams, M. E. K.: 2012c, *MNRAS* **419**, 2163
- Grenon, M.: 1972, in G. Cayrel de Strobel and A. M. Delplace (eds.), *IAU Colloq. 17: Age des Etoiles*, p. 55
- Grenon, M.: 1989, *Ap&SS* **156**, 29
- Guedes, J., Callegari, S., Madau, P., and Mayer, L.: 2011, *ApJ* **742**, 76
- Haywood, M.: 2008, *MNRAS* **388**, 1175
- Haywood, M.: 2012, in *European Physical Journal Web of Conferences*, Vol. 19 of *European Physical Journal Web of Conferences*, p. 5001
- Henry, R. B. C., Kwitter, K. B., Jaskot, A. E., Balick, B., Morrison, M. A., and Milingo, J. B.: 2010, *ApJ* **724**, 748
- Hou, J. L., Boissier, S., and Prantzos, N.: 2001, *A&A* **370**, 23
- Houdek, G. and Gough, D. O.: 2011, *MNRAS* **418**, 1217
- Katz, D., Soubiran, C., Cayrel, R., Barbuy, B., Friel, E., Bienaymé, O., and Perrin, M.-N.: 2011, *A&A* **525**, A90
- Kawata, D. and Gibson, B. K.: 2003, *MNRAS* **340**, 908
- Kazantzidis, S., Bullock, J. S., Zentner, A. R., Kravtsov, A. V., and Moustakas, L. A.: 2008, *ApJ* **688**, 254
- Kobayashi, C.: 2004, *MNRAS* **347**, 740
- Kobayashi, C. and Nakasato, N.: 2011, *ApJ* **729**, 16
- Kobayashi, C., Springel, V., and White, S. D. M.: 2007, *MNRAS* **376**, 1465
- Lagarde, N., Romano, D., Charbonnel, C., Tosi, M., Chiappini, C., and Matteucci, F.: 2012, *A&A* **542**, A62

- Lee, Y. S., Beers, T. C., Allende Prieto, C., Lai, D. K., Rockosi, C. M., Morrison, H. L., Johnson, J. A., An, D., Sivarani, T., and Yanny, B.: 2011, *AJ* **141**, 90
- Lia, C., Portinari, L., and Carraro, G.: 2002, *MNRAS* **330**, 821
- Liu, C. and van de Ven, G.: 2012, *arXiv:1201.163*
- Loebman, S. R., Roškar, R., Debattista, V. P., Ivezić, Ž., Quinn, T. R., and Wadsley, J.: 2011, *ApJ* **737**, 8
- Majewski, S. R., Wilson, J. C., Hearty, F., Schiavon, R. R., and Skrutskie, M. F.: 2010, in K. Cunha, M. Spite, and B. Barbuy (eds.), *IAU Symposium*, Vol. 265 of *IAU Symposium*, pp 480–481
- Martig, M., Bournaud, F., Croton, D. J., Dekel, A., and Teyssier, R.: 2012, *arXiv:1201.1079*
- Martig, M., Bournaud, F., Teyssier, R., and Dekel, A.: 2009, *ApJ* **707**, 250
- Martínez-Serrano, F. J., Serna, A., Domínguez-Tenreiro, R., and Mollá, M.: 2008, *MNRAS* **388**, 39
- Merrifield, M. R.: 1992, *AJ* **103**, 1552
- Meza, A., Navarro, J. F., Abadi, M. G., and Steinmetz, M.: 2005, *MNRAS* **359**, 93
- Minchev, I., Boily, C., Siebert, A., and Bienayme, O.: 2010, *MNRAS* **407**, 2122
- Minchev, I. and Famaey, B.: 2010, *ApJ* **722**, 112
- Minchev, I., Famaey, B., Combes, F., Di Matteo, P., Mouhcine, M., and Wozniak, H.: 2011a, *A&A* **527**, 147
- Minchev, I., Famaey, B., Quillen, A. C., and Dehnen, W.: 2011b, *arXiv:1111.0195*
- Minchev, I., Famaey, B., Quillen, A. C., Dehnen, W., Martig, M., and Siebert, A.: 2012a, *arXiv:1205.6475*
- Minchev, I., Famaey, B., Quillen, A. C., Di Matteo, P., Combes, F., Vlahic, M., Erwin, P., and Bland-Hawthorn, J.: 2012b, *arXiv:1203.2621*
- Minchev, I., Nordhaus, J., and Quillen, A. C.: 2007, *ApJ* **664**, L31
- Minchev, I. and Quillen, A. C.: 2006, *MNRAS* **368**, 623
- Minchev, I., Quillen, A. C., Williams, M., Freeman, K. C., Nordhaus, J., Siebert, A., and Bienaymé, O.: 2009, *MNRAS* **396**, L56
- Mosconi, M. B., Tissera, P. B., Lambas, D. G., and Cora, S. A.: 2001, *MNRAS* **325**, 34
- Moster, B. P., Macciò, A. V., Somerville, R. S., Johansson, P. H., and Naab, T.: 2010, *MNRAS* **403**, 1009
- Navarro, J. F. and Benz, W.: 1991, *ApJ* **380**, 320
- Navarro, J. F. and White, S. D. M.: 1994, *MNRAS* **267**, 401
- Nordström, B., Mayor, M., Andersen, J., Holmberg, J., Pont, F., Jørgensen, B. R., Olsen, E. H., Udry, S., and Mowlavi, N.: 2004, *A&A* **418**, 989
- Oppenheimer, B. D. and Davé, R.: 2008, *MNRAS* **387**, 577
- Pedicelli, S., Bono, G., Lemasle, B., François, P., Groenewegen, M., Lub, J., Pel, J. W., Laney, D., Piersimoni, A., Romaniello, M., Buonanno, R., Caputo, F., Cassisi, S., Castelli, F., Leurini, S., Pietrinferni, A., Primas, F., and Pritchard, J.: 2009, *A&A* **504**, 81
- Peng, C. Y., Ho, L. C., Impey, C. D., and Rix, H.-W.: 2002, *AJ* **124**, 266
- Purcell, C. W., Kazantzidis, S., and Bullock, J. S.: 2009, *ApJ* **694**, L98
- Quillen, A. C. and Garnett, D. R.: 2000
- Quillen, A. C., Minchev, I., Bland-Hawthorn, J., and Haywood, M.: 2009, *MNRAS* **397**, 1599
- Quinn, P. J., Hernquist, L., and Fullagar, D. P.: 1993, *ApJ* **403**, 74
- Raboud, D., Grenon, M., Martinet, L., Fux, R., and Udry, S.: 1998, *A&A* **335**, L61
- Raiteri, C. M., Villata, M., and Navarro, J. F.: 1996, *A&A* **315**, 105
- Reddy, B. E., Lambert, D. L., and Allende Prieto, C.: 2006, *MNRAS* **367**, 1329
- Romano, D., Tosi, M., Chiappini, C., and Matteucci, F.: 2006, *MNRAS* **369**, 295
- Romano, D., Tosi, M., Matteucci, F., and Chiappini, C.: 2003, *MNRAS* **346**, 295
- Roškar, R., Debattista, V. P., Quinn, T. R., Stinson, G. S., and Wadsley, J.: 2008, *ApJ* **684**, L79
- Roškar, R., Debattista, V. P., Quinn, T. R., and Wadsley, J.: 2011, *arXiv:1110.4413*
- Sales, L. V., Helmi, A., Abadi, M. G., Brook, C. B., Gómez, F. A., Roškar, R., Debattista, V. P., House, E., Steinmetz, M., and Villalobos, Á.: 2009, *MNRAS* **400**, L61
- Scannapieco, C., Tissera, P. B., White, S. D. M., and Springel, V.: 2005, *MNRAS* **364**, 552
- Schlesinger, K. J., Johnson, J. A., Rockosi, C. M., Lee, Y. S., Morrison, H. L., Schoenrich, R., Allende Prieto, C., Beers, T. C., Yanny, B., Harding, P., Schneider, D. P., Chiappini, C., da Costa, L. N., Maia, M. A. G., Minchev, I., Rocha-Pinto, H., and Santiago, B. X.: 2011, *arXiv:1112.2214*
- Schönrich, R. and Binney, J.: 2009, *MNRAS* **396**, 203
- Sellwood, J. A. and Binney, J. J.: 2002, *MNRAS* **336**, 785
- Shevchenko, I. I.: 2011, *ApJ* **733**, 39
- Siebert, A., Famaey, B., Binney, J., Burnett, B., Faure, C., Minchev, I., Williams, M. E. K., Bienayme, O., Bland-Hawthorn, J., Boeche, C., Gibson, B. K., Grebel, E. K., Helmi, A., Just, A., Munari, U., Navarro, J. F., Parker, Q. A., Reid, W. A., Seabroke, G., Siviero, A., Steinmetz, M., and Zwitter, T.: 2012, *arXiv:1207.0363*
- Solway, M., Sellwood, J. A., and Schönrich, R.: 2012, *MNRAS* **422**, 1363
- Soubiran, C., Bienaymé, O., and Siebert, A.: 2003, *A&A* **398**, 141
- Spitoni, E. and Matteucci, F.: 2011, *A&A* **531**, A72
- Stasińska, G., Prantzos, N., Meynet, G., Simón-Díaz, S., Chiappini, C., Dessauges-Zavadsky, M., Charbonnel, C., Ludwig, H.-G., Mendoza, C., Grevesse, N., Arnould, M., Barbuy, B., Lebreton, Y., Decourchelle, A., Hill, V., Ferrando, P., Hébrard, G., Durret, F., Katsuma, M., and Zeppen, C. J.: 2012, in *EAS Publications Series*, Vol. 54 of *EAS Publications Series*, pp 255–317
- Steinmetz, M.: 2012, *Astronomische Nachrichten* **333**, 523
- Steinmetz, M., Zwitter, T., and Siebert, e. a.: 2006, *AJ* **132**, 1645
- Stewart, K. R., Bullock, J. S., Wechsler, R. H., Maller, A. H., and Zentner, A. R.: 2008, *ApJ* **683**, 597
- Stoehr, F.: 2006, *MNRAS* **365**, 147
- Tissera, P. B., White, S. D. M., and Scannapieco, C.: 2012, *MNRAS* **420**, 255
- Trevisan, M., Barbuy, B., Eriksson, K., Gustafsson, B., Grenon, M., and Pompéia, L.: 2011, *A&A* **535**, A42
- Villalobos, Á. and Helmi, A.: 2008, *MNRAS* **391**, 1806
- Wielen, R.: 1977, *A&A* **60**, 263
- Wiersma, R. P. C., Schaye, J., Theuns, T., Dalla Vecchia, C., and Tornatore, L.: 2009, *MNRAS* **399**, 574
- Yanny, B. and Rockosi, C., N. H. J. e. a.: 2009, *AJ* **137**, 4377

9. APPENDIX

9.1. The effect of different model realizations

As described in Sec. 2, we have downscaled our simulated disc by a factor of $f=1.67$, so as to place the bar’s OLR just inside the solar circle, at ~ 7.5 kpc (assuming the Sun is at 8 kpc), in agreement with its expected effect on the local disc dynamics (e.g., Dehnen 2000; Minchev et al. 2010).

We now would like to see how our results change if we rescale the disc by a different factor. We use $f=1.4$, which places the solar radius ~ 1.25 kpc inwards of the standard location used in the paper, which is equivalent to having a stronger (longer). We refer to this realization as Model A.

As a second test, we start the implementation with chemistry 2.7 Gyr later, thus avoiding the early massive merger. We integrate the simulation for additional 2.7 Gyr so that we again have 11.2 Gyr of evolution. To keep the correct

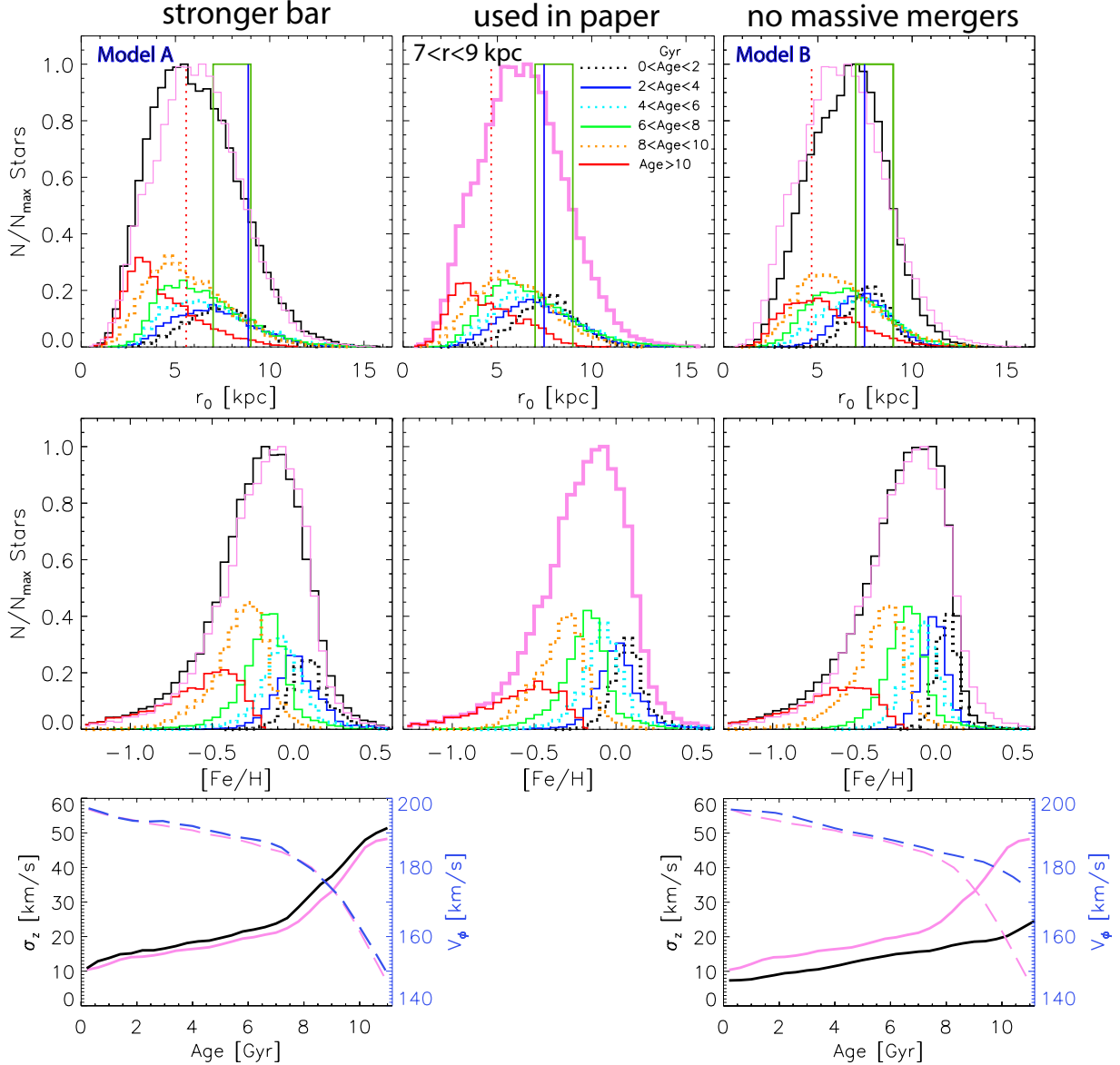


FIG. 12.— Comparison between different model realizations. See text.

location with respect to the bar’s resonances, we downscale the disc radius by $f=2.1$ to account for the bar’s slowing down. This is referred to as Model B.

Note that in both cases above we only change the dynamics but not the input chemistry, i.e., we resample the SFH according to our chemical model, with the 8 kpc chemistry assigned to the rescaled 8 kpc radius in the simulation, etc.

The results are shown in Fig. 12, where in the first two rows we compare the birth-radius and metallicity distributions resulting from our new realizations with $f=1.4$ (Model A, first column) and the time shift (Model B, right column), with our standard rescaling ($f=1.67$, middle column). As expected, when the solar radius is shifted closer to the bar (Model A), a larger fraction of stars of all ages arrives from inside the bar’s CR (dotted-red vertical line in top row); to see this more easily, we have overlaid the original total histogram (in pink) on top of the distributions. Inspecting the metallicity distributions, we see a shift in the peak of 0.1 dex to negative values when the Sun is closer to the bar. However, the changes are not drastic and the rest of the results in the paper are not affected much by this change. Whether this is true for the entire disc will be investigated in Paper II.

As it became evident in the discussion of the age-metallicity relation (Sec. 5.3), in our simulation we have a deficiency of stars with ages > 9.5 Gyr at $r > 10$ kpc. However, this is a very small fraction of particles, as can be inferred from the bottom right panel of Fig. 2 (the SFRs at those times and radii attain a maximum at $\sim 2 \text{ M}_\odot \text{ pc}^{-2} \text{ Gyr}^{-1}$ for $r = 10$ kpc, sharply decreasing for older stars and larger radii). By shifting the solar radius inward, this artifact is now lost. How small this fraction is can be seen by comparing the extent of the red r_0 -histograms (oldest stars) in the first two rows outside the solar bin.

The right column of Fig. 12 shows the new realization with the time shift (Model B), where we have avoided the early-on massive merger, but keep the bar resonances the same distances from the Sun. A smaller number of stars

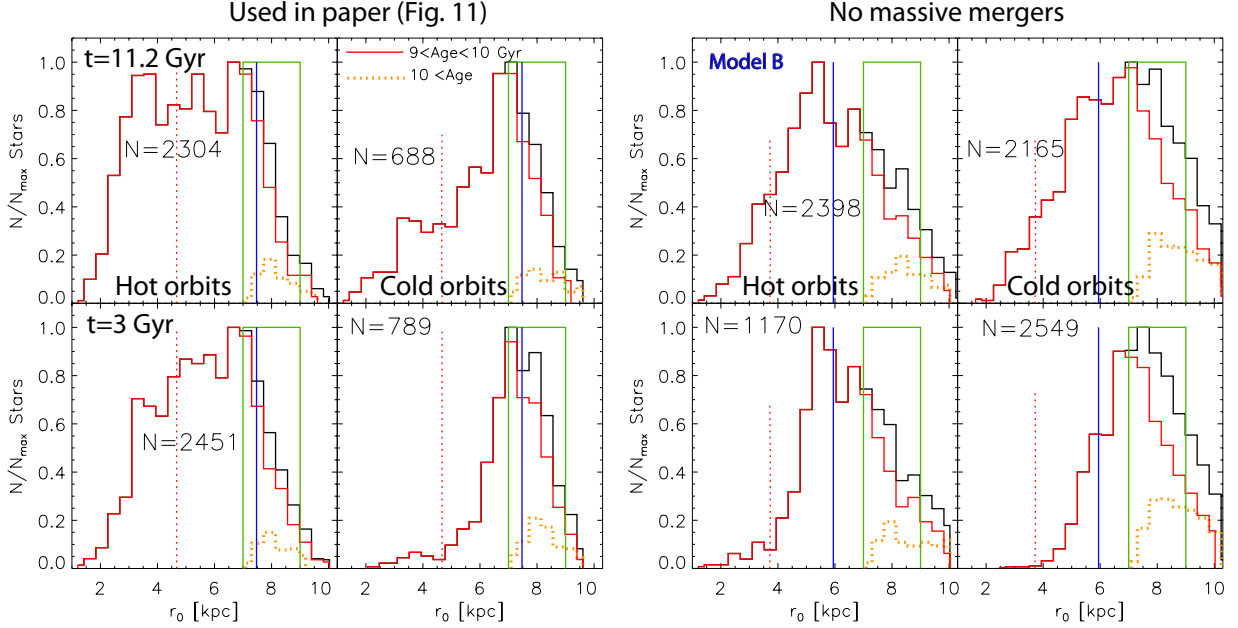


FIG. 13.— Comparison between the effect of an early massive merger (first two columns) and internally-driven radial migration (third and fourth columns) on the dynamics of the oldest stars. See text.

arrives from inside the bar’s CR now, compared to our standard case (see overlaid pink line). This comes mostly from the lack of the strong peak in the r_0 -histogram of the oldest stars (red). We show below (Fig. 13) that the enhancement in the peak at $r_0 \sim 3$ kpc is due to the merger, which we avoid here.

In the bottom right panel of Fig. 12 we compare the vertical velocity dispersion, $\sigma_z(r)$ (solid solid), and rotational velocity, $V_\phi(r)$ (blue dashed), radial profiles resulting from the new realizations with our standard model (pink curves). A slightly larger velocity dispersion is seen for the inner disc radius (left), while the difference is drastic when the massive merger is avoided. Most importantly, the oldest stars have σ_z about a factor of two smaller than when the merger is present. The maximum radial velocity dispersion values (not shown) also drop to ~ 43 km/s, which is reflected in the higher V_ϕ -values. These smaller velocity dispersions and rotational velocity difference between young and old stars is unlike the observed values in the solar neighborhood.

9.2. The effect on the dynamics of the oldest stars in the absence of a massive early-on merger

In Sec. 6.3 we discussed the origin of the old, metal-poor, high-[O/Fe] stars in our simulated solar neighborhood. We showed in Fig. 11 that these stars are born in the range $1 < r_0 < 10$ kpc, where a large fraction is already in place at $t = 3$ Gyr, i.e., shortly after the last massive (1:5 mass ratio) merger ~ 9 Gyr ago.

We now examine the fate of these stars in the absence of a massive early-on merger (Model B in Sec. 9.1). The first two columns of Fig. 13 show the birth radius distributions, r_0 , for the hot (first row) and cold (second row) orbits at the final state (top) and at $t = 3$ Gyr (bottom) for the model realization used in the paper. These are the same as the bottom two rows of Fig. 11. In the third and fourth columns we now plot the equivalent subsamples, but for the model realization lacking any massive mergers (Model B). We first compare the final states (top row). The almost square shape of the distribution for the hot orbits on the left is now replaced by a triangular shape with a maximum just inside the bar’s OLR, i.e., less old stars from the inner disc end up near the Sun when the merger is avoided.

As we showed in Fig. 12, bottom right, for Model B the oldest stellar population has velocity dispersions lower than the standard case. Therefore, separating stars by a cut in eccentricity at $e = 0.2$ results in a “hot” sample with a radial velocity dispersion $\sigma_r \approx 55$ km/s, to be compared to ≈ 65 km/s (on the other hand, both cold samples have $\sigma_r \approx 28$ km/s). The ratio of cold to hot orbits changes from ~ 0.3 to ~ 0.9 . This large difference can be used as a constraint in observations to assess the possibility of an early-on merger in the MW.

Concentrating on the bottom row of Fig. 13 we now see that although it starts with a fully formed bar, Model B is unable to mix the disc by $t = 3$ Gyr as much as in the case of the early-on merger. Only a small fraction of stars arrives from inside the bar’s CR for both the hot and cold orbits.

In conclusion, internally-driven radial migration (compared to the case of an early-on merger) results in (i) a much smaller fraction of old stars originating from $r \lesssim 4$ kpc and (ii) these stars are transferred continuously throughout the disc evolution.

9.3. Migration contribution to the disc velocity dispersions during and after the massive merger

We here shed some light on the effect of migration on the changes in velocity dispersion radial profiles during and after the early-on massive merger in our standard model.

We separate migrating from non-migrating stars (in a given period of time) by applying the technique described by Minchev et al. (2012b). Fig. 14 shows the migrators’ contribution to the disc heating during the merger ($1 < t <$

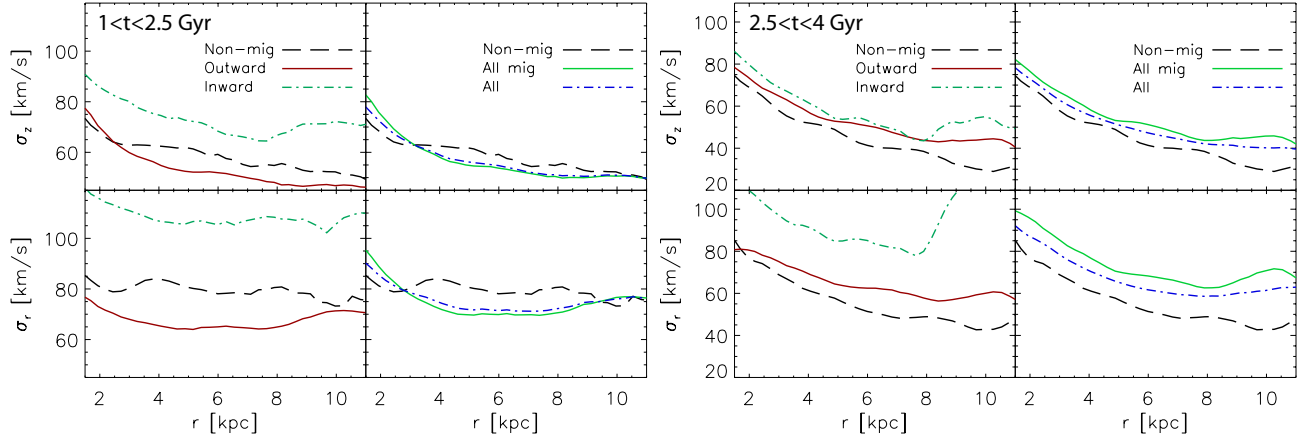


FIG. 14.— Migrators’ contribution to the disc heating during the time period the massive merger takes place (first and second columns) and during a period immediately after that (third and fourth columns). **First and Third columns:** Radial profiles of the vertical (top) and radial (bottom) velocity dispersions, $\sigma_z(r)$ and $\sigma_r(r)$, for non-migrators, outward going migrators, and inward migrators (as indicated) for each time period. **Second and Fourth columns:** The effect of non-migrators, all migrators (i.e., inward and outward going), and the total population. Note that during the merger (left two columns) velocity dispersions are higher for stars coming from the outer disc, followed by the non-migrators, while samples originating in the inner disc are the coolest. This is due to the stronger merger effect on the outer disc. In contrast, at later times (right two columns), the bar and spirals transfer the already preheated stellar populations, thus, contributing to disc heating.

2.5 Gyr, first and second columns) and during the time period immediately after that ($2.5 < t < 4$ Gyr, third and fourth columns). The radial profiles of the vertical (top) and radial (bottom) velocity dispersions, $\sigma_z(r)$ and $\sigma_r(r)$, for non-migrators (dashed black curve), outward going migrators (solid brown curve), and inward migrators (dash-dotted green curve) for each time period are shown in the first and third columns. The second and fourth columns show the effect of non-migrators (dashed black curve), all migrators (i.e., inward and outward going, solid green curve), and the total population (dashed-dotted blue curve).

During the merger (left two columns) velocity dispersions are higher for stars coming from the outer disc, followed by the non-migrators, while samples originating in the inner disc are the coolest. This behavior (especially for σ_z) is opposite to the effect expected from internally-driven migration (Minchev et al. 2012b) and is due to the stronger perturbation experienced by the outer disc, given its exponential surface density decrease. The second column shows that, for $r \gtrsim 3$ kpc, the overall effect of migrators is to decrease the total velocity dispersion, because most migrators come from the inner disk.

In contrast, at later times (right two columns), migration induced by the bar and spiral structure transfers out the already *preheated* stellar populations, thus, contributing to disc heating. As the disc grows further from gas accretion, this contribution becomes much smaller. The weak effect of migration on disc heating at the later stages of this same galaxy evolution was presented in Fig. 8 (model C3) by Minchev et al. (2012b).